Compression Device for 3D Spheroids in Microgravity

ME450 Section 4 Team 14 - Winter 2021

Zach Bultsma, Rohan Dalvi, John Radke, Sean Van Note

University of Michigan - Department of Mechanical Engineering
Sponsor: Grace Cai
Mentor: Dr. Allen Liu

April 27, 2021

Table of Contents

EXECUTIVE SUMMARY

The foundation of this project is to assist in furthering the understanding of the degenerative bone disease osteoporosis. This disease causes bones to become weak and brittle, potentially resulting in a fracture of the bone from a mild stress. Osteoporosis can be caused by a variety of factors but the one used as the primary basis behind the project is having a sedentary lifestyle, or lack of use. This is a problem that also applies to astronauts in space. With extended periods of time suspended in weightlessness, astronauts do not have the load of gravity on their bodies, mimicking the effects of a sedentary lifestyle on earth. This leads to astronauts developing osteoporosis that is in some cases worse than others on earth [1]. Research was conducted to further the team's understanding of the subject and how engineering design may help in furthering our knowledge of osteoporosis.

The need to counteract the bone loss faced by astronauts starts with confirming the hypothesis that a mechanical load applied to the bone will help prevent it. Thus, a compression device must be designed that enables the study of the effect of compression on bone cells while in microgravity conditions. Previous research and designs of devices that compress bone cells are plentiful. Examples of designs are discussed at length within the research section of this report. These designs further the team's understanding of the design space that we are able to operate in when designing our device.

The requirements of our design were determined from an interview with a member of the University of Michigan ME Liu Lab, Grace Cai, a PhD student and the Lead Sponsor of the project. Cai described the desired environment of the test, and a myriad of other design requirements. A quantitative and measurable set of engineering specifications were determined to satisfy the requirements from conditions of the test, and the functions provided from the company partnered with the Liu Lab, Space Tango.

Brainstorming sessions that explored the design solution space resulted in concept generation. From the myriad of concepts, each concept was categorized based on subfunctions of the device. Each concept generated was evaluated through various concept evaluation techniques. Concepts that did not pass any of the evaluations were not considered for the final device design.

CAD design, computational modeling, and hand calculations were done on the design to ensure all specifications are met. Our final device design, verification, assembly procedures, and bill of materials are completed and documented. A critique of the final device design was made to document the strengths, weaknesses, and risks of the design so that potential design improvements could be made if need be. Furthermore, our team included a detailed description of project context assessment, a discussion on how our team conducted engineering inclusivity, how our team made environmental considerations, and how our team made ethical decision making when designing our device.

We have completed the preliminary design work that is required to ensure a design that meets sponsor requirements. We appreciate the collaboration we have had with Grace Cai, Liu Lab, and Space Tango. The contents of this report pertain to Design Review 1-3, and Final Solution and Project Report. This report details our design problem background and definition, research, requirements and specifications, concept generation and evaluation, final design, engineering analysis, design verification, critique of design, current project status, project context assessment, environmental design considerations, engineering ethics, and team engineering inclusivity practices.

PROBLEM DESCRIPTION

Osteoporosis is a degenerative bone disease that can lead to frail bones due to decreased bone density. As seen below in Fig.1, the bone structure becomes more porous, resulting in bone structural integrity being compromised. This can lead to a host of medical issues such as bone fracture, and in 2020 it was estimated that more than one in two Americans over the age of 50 will be at risk or develop osteoporosis [2]. There is no cure for osteoporosis, and current treatments typically aim to mitigate the risk of severe injuries via medication.

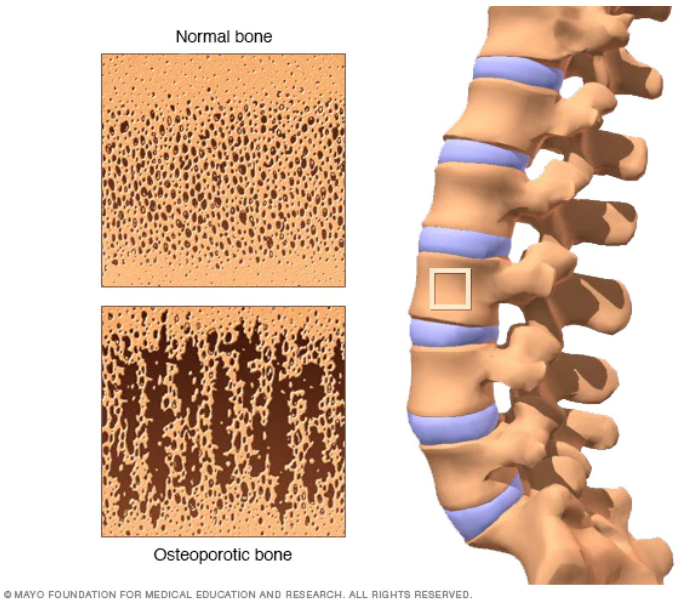

Figure 1: Demonstration of loss of bone density caused by osteoporosis [3].

Through previous research on 2D breast cancer cell compression, Liu Lab wants to test whether a compressive load on spheroids (3D aggregates of cells) of osteoblasts (cells responsible for bone structure architecture) could yield more efficient cell function. Spheroids are to be used rather than 2D structures as they are more reflective of cell physiology such as tissue architecture

and cell dynamics [4]. While in the microgravity of space, the spheroids will artificially exhibit symptoms of osteoporosis, and after a period of time, will be compressed statically or cyclically at 0, 600, 1200, or 1800 Pa for 24 or 72 hours. The scope of this project is to design and fabricate the device that compresses these spheroids while on the International Space Station. The spheroids will be embedded within a collagen gel. The cells will be compressed indirectly, but the gel will be compressed directly. As the gel is compressed from our device, the cells are compressed from the gel compression. Our device will be situated within a CubeLab, which is a small scaled box that accommodates a variety of scientific experiments. The CubeLab will offer a compartment in which our device will reside for experimentation and power to any device actuators.

EXISTING RESEARCH

Elaboration of the existing research is useful in demonstrating the need for further experimentation. This section discusses research on the effects compressive loading on bone cells and micro-devices that provide load on cells. Examples of such devices are explained in detail.

Studies on Compressive Loads on Cells

The study of compressive loads on bones has a long history spanning centuries into the past. In particular to the project at hand, there are a plethora of research documents pertaining to a lack of compressive load on bones. Within the ISS and within space more generally, gravity does not exert the same force as it does as on Earth. Human bone structures have evolved under constant compressive loads from gravity. Without compressive loading, the human body does not provide the biochemical reactions necessary for the promotion of bone growth. This idea is further elaborated upon by Damian Genetos of Pennsylvania State University in their thesis on Cellular and Molecular Physiology, states:

“For bone to best serve as a weight-bearing organ, its architecture must be modified to adequately address changes in structural demand. Increased stresses, or loads, on bone must be compensated with bone formation, whereas decreased stresses on bone should reduce bone mass to prevent wasted energy expenditures. A plethora of data support this idea, known as Wolff’s Law. The microgravity conditions of spaceflight are one such example of a condition resulting in diminished skeletal loading.” [5]

As Genetos points out, the overall mass of bone is forever changing based on bodily needs. The maintenance of bone structures require compressive loading to promote bone formation over bone reduction. A long term example of a lack of loading on bones are applicable to members of the ISS, as many members are in space for months to years per mission. This lack of loading causes astronauts to be susceptible to osteoporosis and bone fractures after returning from

missions. Saini Vilkas of The University of Chicago in their thesis on Pulsed Ultrasound and Shear Stress Interact in Their Regulation of Bone Cell Morphology and Function, states:

“Whether bone tissue is formed or resorbed is determined by whether there is an increase or decrease in the loading regime experienced by the bone.” [6]

An additional concept that ties into Wolff’s law and the issues that spaceflight cause on ISS members is mechanotransduction. Within our problem proposal given from Liu group in collaboration with the Center for Advancement of Science in Space (CASIS), states that Liu group are examining cellular mechanotransduction of human osteoblasts on the ISS. To further illustrate mechanotransduction is a quotation from Aaron Weaver of The University of Michigan in their thesis on The Effect of Mechanical Stimulation on Bone Fracture Healing, stating:

“Mechanotransduction is the means by which a mechanical signal is sensed and converted into a biochemical reaction. Since the late 1800's, when Julius Wolff proposed that the form of bone follows its function, it has been postulated that bone is responsive to mechanical cues.” [7]

The biochemical reaction stated above in Weaver’s statement is a reaction that either aids or inhibits bone tissue formation. A lack of compressive loading on ISS members inhibits the necessary mechanical signals that the body uses to cue biochemical reactions for bone formation. Furthermore, a lack of compressive loading does not allow the bone to follow its natural functions. When bones are subjected to natural functions caused from compressive loading, there are side effects to the bone that are pointed out by Danese Joiner of The University of Michigan in their thesis on The Effect of Age on Bone and its Response to Mechanical Stimulation. Joiner states that:

“Mechanical stress improves bone strength by influencing collagen alignment as new bone is formed and daily loading can result in increased bone formation rate, bone mineral apposition rate, and labeled bone surface area.” [8]

As from these benefits, a bone will be stronger under compressive loads than without load. The overall strength of bone to resist fracture is dependent on its mass, geometry, and other intrinsic properties to bone. Without load, the reduction of newly made bone tissue or osteoblasts will adjust bone geometry and mass based on the current load bearing needs. This is because the body optimizes energy usage by only producing enough osteoblasts to balance bone mass and geometry for adequate strength of the situation.

As for people that are under microgravity conditions, the bone structure of those people’s bodies will weaken. This phenomena will as a result impact the physiology of bone cells within people experiencing microgravity conditions for prolonged periods of time. As conditions of space

travel and space colonization become more realized, interest in the phenomenon of physiological changes to the human body under microgravity conditions has been made apparent. As the Liu group examines compressed osteoblasts on the ISS, the results obtained from the research may yield important information on the nature of compressed bone cells under microgravity conditions.

Studies on Devices That Mechanically Load Cells

As it becomes more feasible to design micro-scale mechanical devices, the ability to design devices that load bone cells also become more efficient. Within the past quarter century, there have been several examples of micro-scale devices that facilitate load on bone cells. Multiple loads, either static or oscillatory, can be used during testing of cells. Furthermore, devices that provide loads have been designed that are comparable to the scope of the current project definition.

There are three previously designed load actuating devices that will be shown to illustrate how such devices work and the applicability of such devices to this specific project. As will be discussed more thoroughly within the specifications and requirements section of the report, there are basic stakeholder requirements that our design must fulfill. Our device and the devices that will be shown in the succeeding paragraphs will share some of the same basic requirements. The basic requirements that will be compared will be that both classes of devices must: first, circulate cell media through cell compartments; second, provide micro-loads to cells; and third, be able to be actuated automatically by computer.

General loading device on cells

The first device shown will be a device that provides multiple loads on bone cells at the same time. This device will be more of a general example illustrating that complex designs that actuate multiple loads on bone cells have been achieved in the past. Saini Vilkas of The University of Chicago in their thesis on Pulsed Ultrasound and Shear Stress Interact in Their Regulation of Bone Cell Morphology and Functions, designed a device that provides multiple loads on bone cells. Their design, shown in Fig. 2 [6], cultures bone cells on a plate at the top-middle section of the figure, left of the vibration shaker.

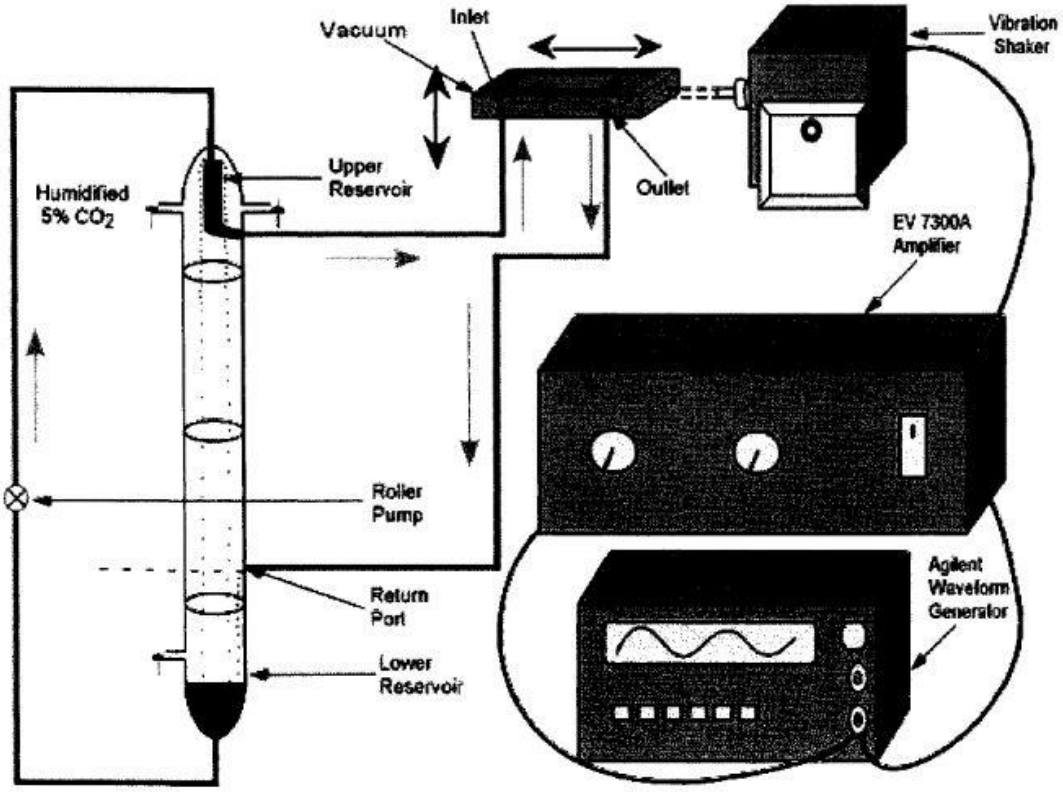

Figure 2: Design that actuates laminar fluid shear stresses and oscillatory ultrasound stresses [6].

For the design shown in Fig. 2, bone cells were subjected to to a known shear stress of 19 $\frac{dynes}{cm^2}$ (1.9 Pa) from the cell media from the inlet to the outlet of the cell parallel plate chamber. Additionally, the bone cells were subjected to oscillatory loads from the vibration shaker. The vibration shaker provided a frequency of 200 or 400 Hz and a 1 $\frac{mm}{s}$amplitude. The shaker was controlled by a programmable arbitrary function generator and power amplifier.

The design shown in Fig. 2 and our design will now be compared. For reference, our design conditions are discussed within the Requirements and Engineering Specifications section of the report. Some conditional similarities between the design shown in Fig. 2 and our design are: first, the temperature of both testing environments vary by 4 ℃; and second, both devices allow cells under experimentation to be infused and humidified with 5% CO_2 [6]. The device shown in Fig. 2 is a general example of a device that can provide micro-loads to bone cells while also satisfying basic stakeholder requirements. The device aforementioned does not actuate a dominant micro-compressive load required for our purposes. However, the principles from the device provide useful information on how to provide any number of stresses on bone cells, including compressive stresses. The next two designs discussed that promote compressive loads to cells are quite similar to this design in principle. A few key design changes to the flow plate to

promote compressive loads is the main difference between this design and the next two discussed designs.

Microfluidic loading device on cells using air

Examples of devices that actuate compressive loads to bone cells are plentiful and have been explored thoroughly. Using microfluidics within a mechanical device can cause actuated compressive loads to breast epithelial cells. Microfluidic devices manipulate the properties of fluid mechanics at micro-scales to achieve certain types of micro-loading. Kenneth Ho of the University of Michigan in their Thesis of Progressing Mechanobiology from a Simplified to a More Complex System: Development of Novel Platforms and Investigation of Actin Cytoskeletal Remodeling, has designed a variation of a microfluidic device that provides compressive loads on cells. Their design, as shown in Fig. 3 [9], has a compressive chamber in which cells reside.

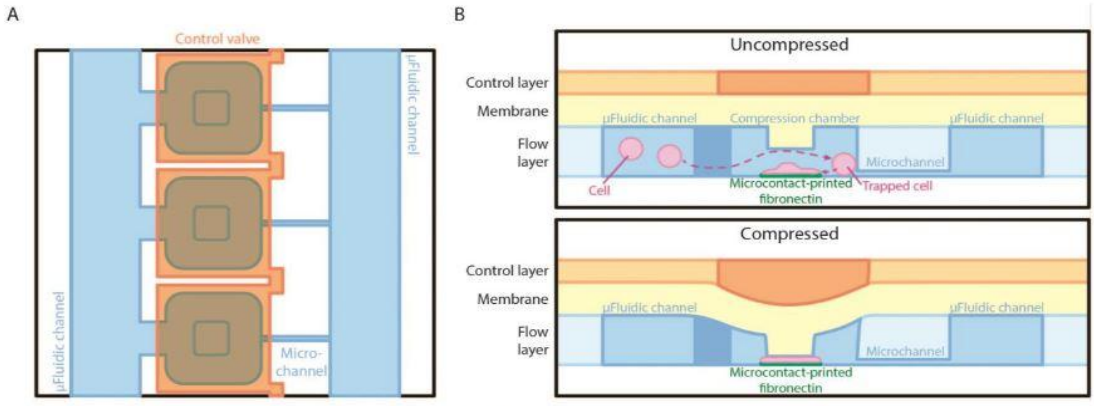

Figure 3: Schematic showing the design of a microfluidic device. (A) A top view of the flow layer and control layer design at the compression chamber. (B) A side view of the microfluidic device when the control layer was uncompressed (top) and compressed (bottom). [9]

For the design shown in Fig. 3, the control layer was constructed with PDMS, a commonly used polymer with an elastic modulus of 0.3 MPa, a Poisson's ratio of 0.49 and a density of 970 $\frac{kg}{m^3}$. The control layer is compressible by an external load. The external load used was air pressurized at 5, 10, and 15 psi [9]. When the control layer is deflected from the external load, the cells within the compression chamber are compressed and subsequently strained. In knowing material properties of PDMS and the usage of CAD, FEA, and CFD programs, the deflection of the control layer and pressure within the compression chamber is theoretically known. From experimental and theoretical analysis on cells within the device, the strain on cells can be found. An example of cells compressed from the microfluidic device is shown in Fig. 4 [9]. From the figure, the strain on the cells can be found at any given external loadings that were tested upon. For reference of design scale, the compression chamber width is 80 μm. Based on the scale given

and the regulated external load on the control layer, the compression and strain on the cells themselves are at microscale.

This device is applicable to our device that will be designed for a few reasons: first, cell media can flow through the compression compartment while the cells are tested upon; second, the external force and media flow can be actuated from a computer without any human interface; and third, based on Fig. 4, the strain on the bone cells are within appropriate ranges for the scope of the project. However, there are many applications of microfluidics that apply compressive stresses to bone cells using designs that vary external load delivery to the control layer and or internal fluid state properties to achieve desired experimental results.

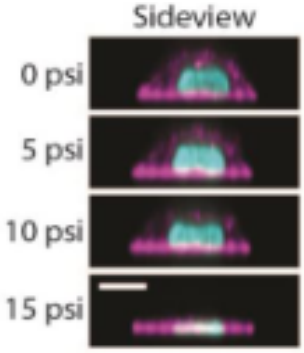

Figure 4: Side view of bone cells compressed from varying external loadings on the control layer. Scale bar = 10 μm [9].

Microfluidic device loading cells using water

Another example of a design that compresses cells is the following application of a microfluidic device. Yu Chang Kim, et al. of the Korea Advanced Institute of Science and Technology (KAIST) in their scientific paper on: Microfluidic biomechanical device for compressive cell stimulation and lysis, devised a microfluidic design that compresses MCF7 cells. As shown in Fig. 5 [10], the authors made a flow channel design that congregates cells to the floor of the channel so that the cells would not flow outside of the channel along with the cell media. Cells are compressed using an external load delivery to the flow channel. Water within a control panel is pressurized using an actuator causing the PDMS membrane to deflect the flow channel. The compressive load is applied to the cells through the deflected PDMS membrane between two microchannels [10].

The end goal of the aforementioned authors of the device required a much higher applied compressive stress to the cells. Under the test conditions, the cells tested had applied compressive stresses ranging from 10 to 35 kPa. The design shown in Fig. 5 and our design will now be compared. For reference, our design conditions are discussed within the Requirements and Engineering Specifications section of the report. Some conditional similarities between the design shown in Fig. 5 and our design are: first, the temperature of both testing environments are within 5 ℃ of each other; second, both devices allow cells under experimentation to be infused with 5% CO_2; and lastly, fluid flow within the flow and control channels a can be automatically activated from a computer [10]. Even though the MCF7 cells tested are not bone cells, the principles used within the device are applicable to our design. Furthermore, it is within the scope of the project to be able to apply an external load from pressurized water at a much lower pressure than shown in the example design.

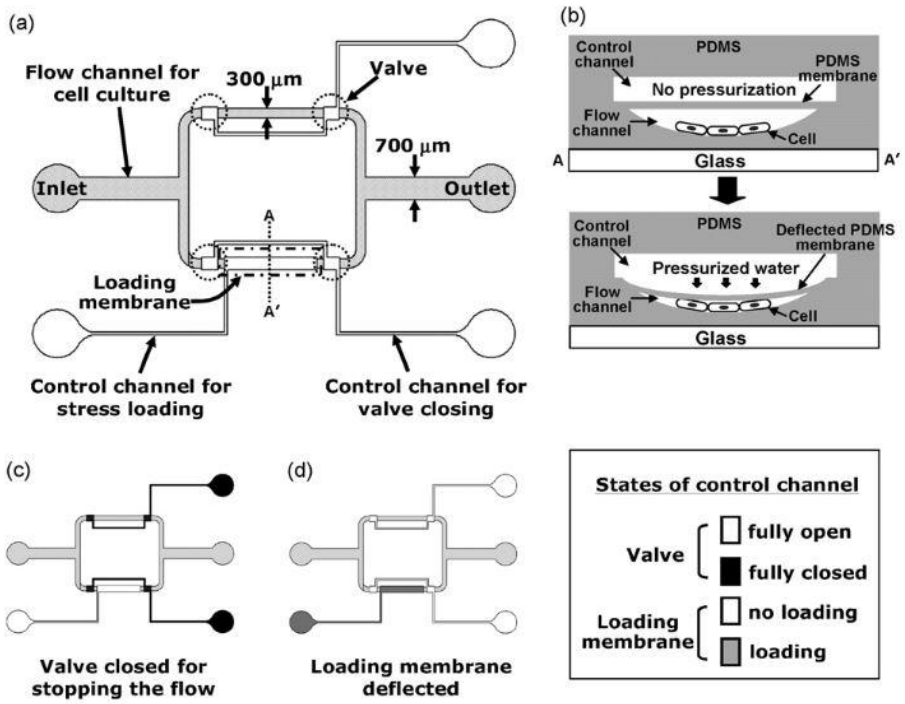

Figure 5: Schematic of the microfluidic device. (a) Top view of the microfluidic device. Two parallel channels segmented are one (lower) for application of the stress and the other (upper) for comparison. (b) Cross-sectional view of the device (dotted line A–A′of (a)). Schematic of the operation of the control channel. (c) Fouron-chip valves are used for locking up the cells in microchannels and facilitating cell attachment. (d) When the valve is open, it is possible to compress the cells through the direct contact with the deflected membrane. [10]

REQUIREMENTS AND ENGINEERING SPECIFICATIONS

User requirements were largely determined from conversations with our primary sponsor, Grace Cai, with several additional guidelines set by Space Tango and NASA. These requirements were then developed into engineering specifications that could be evaluated empirically. To better demonstrate each stakeholder's role in the overall experiment, the requirements and specifications have been split into two tables: experimental requirements (Table 1), and environmental requirements (Table 2). Experimental requirements are those in relation to the spheroids and their compression in the CubeLab, while environmental requirements are those which are related to constraints set by Space Tango and NASA, which are largely logistical and facilitative in nature.

Table 1: Experimental requirements and engineering specifications.

Requirements	Specifications
Device must test a series of cells within individual cell compartments	Cells within 4 rows and 4 columns of cell compartments Cell compartment volume: 1 mL
Device must circulate fluids throughout cell wells	Cell media flow rate: 3.2 mL / min
Device must be permeable to CO_2	Cells must have contact with 5% CO_2
Device must pressurize cells within gel	Facilitate Strains of 10, 20, 30% on spheroids Static loading for a duration of 24 or 72 hours Cyclic loading for 30 minutes on and 30 minutes off for a duration of 24 or 72 hours
Must partially vacate media from cylinders to avoid pressure build up from compression	Media must partially vacate all cylinders within 1 minute of initiated compression
Do not use materials that react with or damage the gel or cells	Use 3D printed resin, PDMS, and glass in direct contact with gel or cells Use metals, stainless steel, and or glue that do not contact with gel or cells Materials used must be resistant to ethanol Materials compliant with NASA guidelines

The experimental requirements were developed into engineering specifications by taking into account priorities, prior experimentation, and interviews with Cai. The CO_2 level of 5% and the material restrictions are justified as biological necessities of the spheroids. The other specifications facilitate Cai's experiment design. The volume and configuration of the cell wells were predetermined by Cai. Using these, and Cai's request that the fluids circulate throughout the entire device in roughly 5 minutes, we determined the flow rate of 3.2 mL/min, but is subject to change and is relatively flexible. The static and cyclic compressive volumetric strains of 0 10, 20, and 30% came from prior experimentation on spheroids on Earth. Media must vacate all cylinders within 1 minute of initiated compression because during compression we do not want the compression to create a media pressure build up within the cylinders.

Table 2: Environmental requirements and engineering specifications.

Requirements	Specifications
Device must fit in CubeLab Box	Device Dimensions of 127 mm per axis
Device must withstand environment in transit to ISS and the ISS itself	Device can withstand at least 10 trial runs Can stay intact for 7 days in space pre-test Temperature of cells must be at 33.5 C +/- 1C
Device must be compatible with automation capabilities of Space Tango	Device must be capable of being driven by a laptop via USB connector

The environmental specification values and procedures were primarily determined by Space Tango and NASA. The CubeLab itself has standardized dimensions, and the temperature within can be specified via CubeLab's internal thermal control. The automation compatibility is likely a

requirement and specification that will be changed as our team communicates further with Space Tango and better understands how our device and the CubeLab can be integrated.

CONCEPT GENERATION

From our previous sections the project problem and requirements are now fully defined; thus, the ideation process will begin. Our team first started with dividing the device into two main sub functions: compression, and media flow. Each sub function will have multiple components and will be combined with other subfunctions to constitute the whole device. As such, each sub-function must work with one another to ensure the device's functionality.

Concepts were initially generated through broad scoped brainstorming sessions. These sessions, lasting roughly a half hour long, allowed our team to freely exchange a range of diverse ideas. Our most broad questions that we explored the solution space were: "What channels fluid flow?", "How can fluid enter cell containers?", "How are forces actuated?", and "What forces can cause compression?". By combining ideas that were generated independently and as a team we were able to build upon each other's ideas. Furthermore, by suspending judgment on the ideas that were brought up within the sessions, our attitudes were much more lax. Suspending judgment also adds more diverse points of view within the sessions because most people are more creative when the fear of rejection is not present.

Methods of Compression

As a result of the brainstorming sessions, our team created fifteen concepts that are within the solution space. All pictorial representations of our concepts are shown in Fig. 6 through Fig. 11.

As shown in Fig. 6, the fluid pressure actuation concept would be paired with the piston/cylinder housing concept. A floating piston would reside within the cylinder. Initially the chamber above the piston is without fluid flow, so within microgravity conditions the piston would remain static. Fluid flow within the chamber above the piston would cause a downward force on the piston. This downward force would cause a compressive force on the cells.

As shown in Fig. 6, the solenoid actuation concept would be paired with the piston/cylinder housing concept. A piston would be connected to the shaft of a solenoid. When actuated, a solenoid will push the shaft downward, which will push the piston downward. The downward push of the piston will generate a compressive force on the cells.

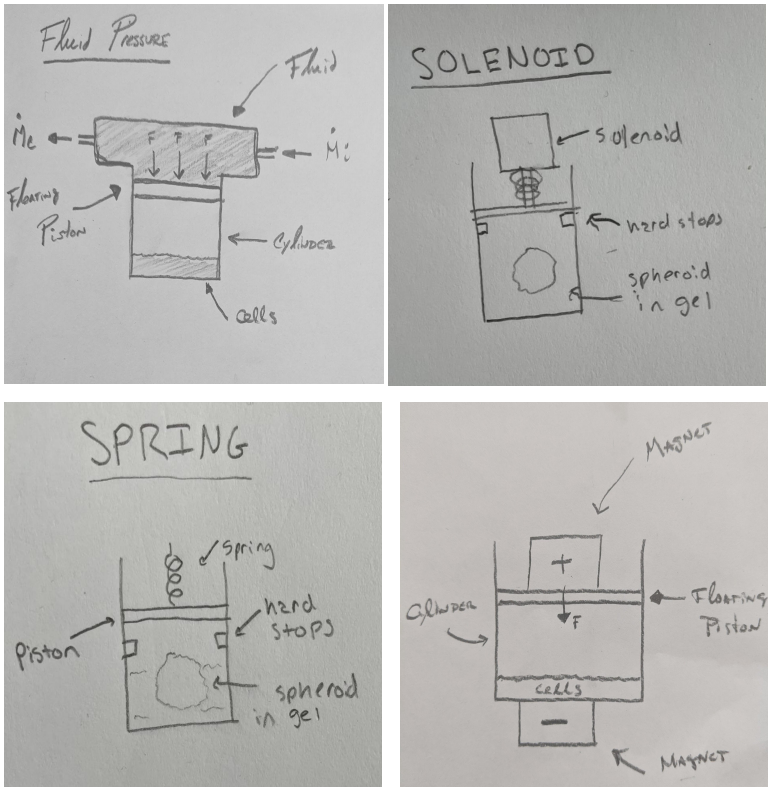

Figure 6: A set of four brainstormed ideas using a piston/cylinder. Clockwise from top left: fluid pressure, solenoid, magnet, and spring actuation.

The magnet-actuated concept would be paired with the piston/cylinder housing concept. A floating piston would have an electromagnet mounted above. An additional electromagnet would be mounted below the cylinder. When both electromagnets are supplied current and have an opposite polarity, an electromagnetic attraction force is created between both electromagnets. The attraction force would push the piston in a downward direction, which would generate a compressive force on the cells.

The spring-actuated concept would be paired with the piston/cylinder housing concept. A piston would be connected to a pre-sprung spring. When the spring is un-sprung, the spring would extend its length in a downward direction, which would push the piston downward. The downward push of the piston would generate a compressive force on the cells.

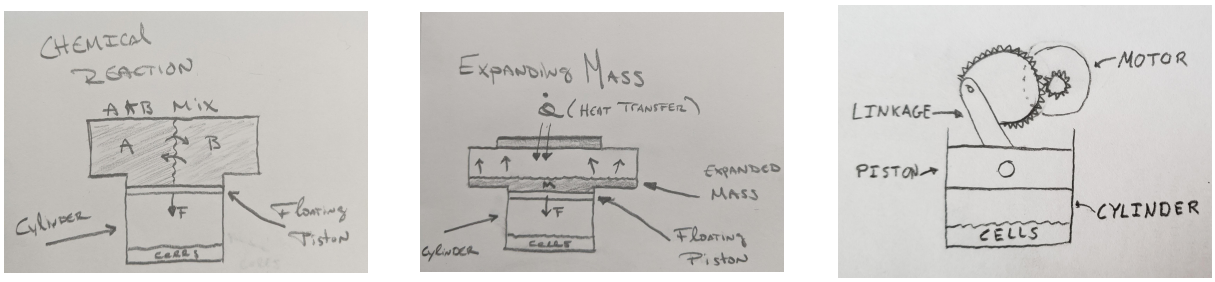

Figure 7: A set of three brainstormed piston/cylinder actuation concepts. From order of left to right: chemical reaction, expanding mass (foam), and motor with linkage.

The chemical reaction concept would be paired with the piston/cylinder housing concept. This would involve a chemical mixture of different solutions and floating piston. When the solutions are mixed it would create pressure that in turn pushes the floating piston down.

We also thought of using a foam that would expand when applied with heat. Similar to how the chemical reaction applied pressure, the expansion of the foam would push the piston down and create the necessary pressure on the cells.

The last piston/cylinder concept we came up with was using a motor and linkage. Utilizing a linkage we could convert the rotational motion from the motor to a linear motion, allowing us to push the piston down. This is because the piston is constrained to one degree of motion, up or down. A four bar linkage would be needed to convert to the correct motion where one link is rigidly attached to the output shaft of the motor, another link being freely attached to the first link and piston, then the piston cylinder would act as a third link, and then a ground link.

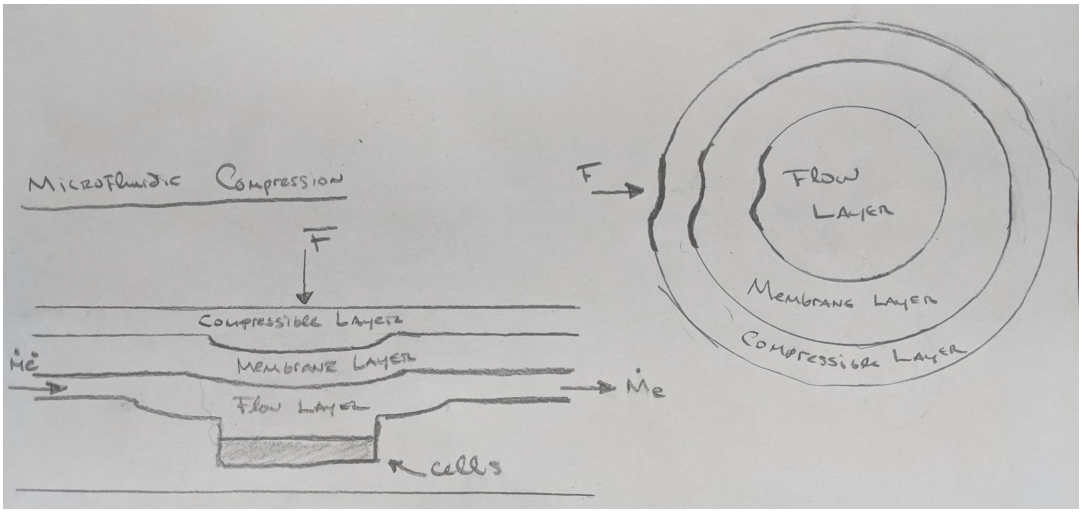

Figure 8: A pictorial representation of microfluidic compression.

The microfluidic compression device has three layers: a compressive outer layer, an intermediate membrane layer, and a media flow layer. To compress cells within the flow layer, an external force is applied to the compressible outer layer to deform both the compressive and membrane layers, which as a result deforms the flow layer. The deformed flow layer has a smaller total volume than before with the same initial media flow rate. As a result, the pressure of the flow layer will increase, which will provide a compressive force on the cells.

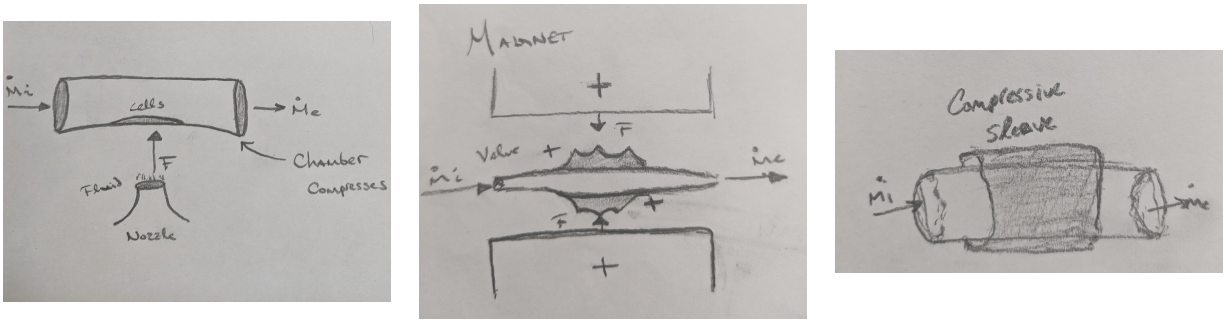

Figure 9: A set of four brainstormed ideas using microfluidic compression. From order of left to right: fluid pressure, magnet, and compressive sleeve actuation.

The fluid pressure actuation would be matched with a microfluidic compression device. Fluid would be released through a nozzle to generate the external force needed to deform the compressive layer.

The magnetic actuation would be matched with a microfluidic compression device. Two electromagnets would be mounted above and below the compressive layer. The exterior of the compressive layer would have a positively charged coating. When both electromagnets are supplied current and have a positive charge, an electromagnetic repulsion force is created between both electromagnets and the compressive layer. The repulsion force would deform the compressive layer, which would generate a compressive force on the cells.

The compressive sleeve would be matched with a microfluidic compressive device. An empty sleeve with an inlet valve will surround the compressive layer. When fluid enters the sleeve through the inlet valve, the pressure within the sleeve will increase; thus, the sleeve will expand in all directions. The expansion of the sleeve will deform the compression layer, which would generate a compressive force on the cells. This design is analogous to a blood pressure cuff used in a doctors office.

Methods of Media Flow

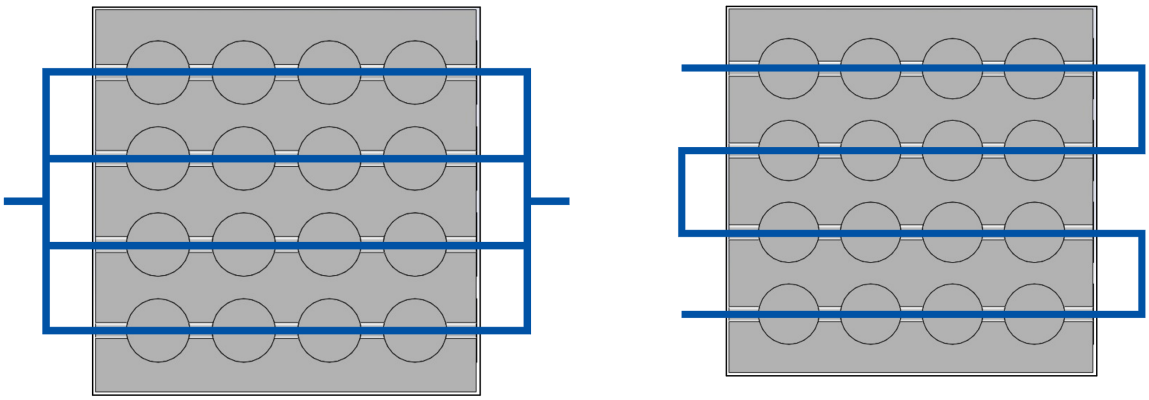

Figure 10: A set of two channel concepts for media float. The left shows parallel channels and the right uses series channels.

With one of our requirements stating that we have to flow media through our device combined with a 4x4 cylinder design, we brainstormed two different ways we could get media to each well. One of these ideas was using parallel channels. This uses a branch or splitter where the hose from the media storage splits, allowing a channel for each row. This is similar to a parallel circuit in electronics where the voltage is constant, but in our case the media flow would be constant. Both channel concepts will use an inlet valve to regulate media flow rate to the amount specified within our engineering specifications.

Another channel design we brainstormed was using a series channel. This is where the media would enter at one point and would travel through all 16 cylinders in series before it exits. While the parallel channels are similar to parallel circuits, the series channel would compare to a series circuit with one entrance and exit for our device.

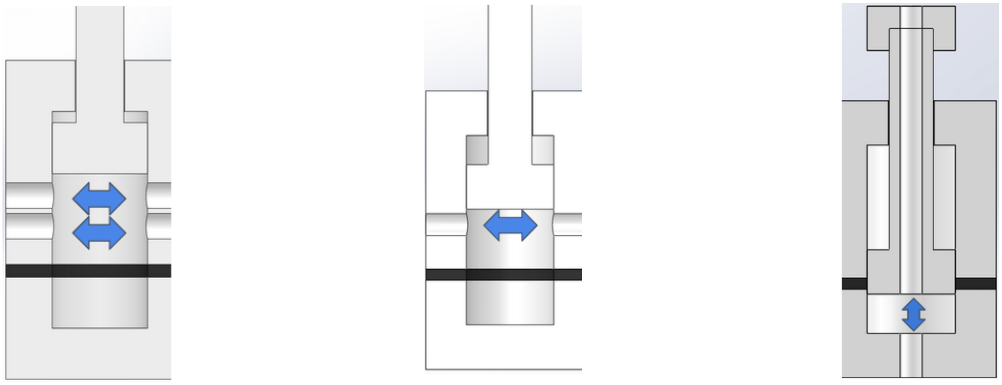

Figure 11: A set of flow orientation concepts. In order of left to right: multi-channel flow, horizontal flow, and vertical flow.

After brainstorming the different channels we could use we then focused on the orientation of the flow. One of these concepts was using a multi-channel, in other words, multiple holes. The idea behind this being we could easily control whether that be laminar or turbulent flow. We then narrowed down the orientations to be either horizontal or vertical flow. Horizontal media flow is perpendicular to the line of action of the piston, as shown in the middle figure within Fig. 11. Vertical media flow is parallel to the line of action of the piston, as shown in the right most figure within Fig. 11.

As a result of concept generation, fifteen concepts were produced. Each concept provides a specific function that would be utilized by the final design concept. As such, each of the specific functions were categorized into subfunctions. Using a morphological chart as shown in Table 3, concepts can be categorized by a specific subfunction.

Table 3: Morphological chart of the brainstormed concepts.

Sub Function	Solutions									
Compression	Piston/Cylinder Compression	Motor with linkage	Spring	Solenoid	Magnet	Fluid pressure	Expanding foam	Chemical reaction	Microfluidic compression	Fluid pressure from compression sleeve
Media Flow	Vertically fed orientation	Side fed orientation	series channels	parallel channels	Multi-channel					

CONCEPT EVALUATION

Following the concept generation phase, our group categorized each concept generated into one of the four sub functions using a morphological chart, and into organizing principles. After categorizing each concept, we discussed and voted on the pros and cons of each concept to narrow down the concepts for each sub function. To do this step, our group used concept evaluation techniques in the order of: feasibility judgment, technology readiness, and Pugh charts. Through these techniques our group found the most robust concepts to our requirements and engineering specifications. These remaining concepts will be considered when selecting a final design.

A feasibility judgment eliminates concepts that are deemed non-feasible under any circumstances. Concepts were rated as feasible, conditionally feasible, worth considering, and not feasible. Based on our requirements and specifications, we imposed constraints on our concepts. The constraints are shown on Table 4. For a concept to be considered, the concept must abide by all constraints. If a concept fails any constraint, that concept will not be considered as a feasible solution. Constraints are based on the requirements and specifications of the project. A feasible concept passes each constraint without any or minimal concern. A conditionally feasible concept is a concept that is feasible if additional information is found, such as research. Concepts that are worth considering are neither good nor bad based on feasibility judgments. Any concept

that is not feasible will not be considered for further evaluation. Any concept other than a not feasible concept will be considered for further evaluation.

Table 4: List of imposed constraints used on concepts during feasibility check.

	Constraints
1.	Zero Gravity
2.	Small-scale design (dimensions)
3.	Manual assembly
4.	Manufacturable
5.	Repeatable/Precise applied compressive force (w/in 5% of target)
6.	Closed system
7.	Compatable with Space Tango electronic/mechanical equipment
8.	Reliable; works after many tests
9.	Constant temperature
10.	Must manually access cells before and after testing
11.	Conducive to media flow

A technology readiness assessment determines our team's readiness of the technologies used for the concept. Concepts were evaluated based on the following four questions: "Do reliable and reasonable manufacturing processes exist?", "Do appropriate material choices for the solution exist and are they readily available?", "Does our team have sufficient technological expertise for the solution considered?", "Do similar applications exist that demonstrate the technology's readiness?". Concepts were rated as "yes", "possibly, "questionable", and "no" when evaluated upon. Concepts rated as a no to any of these questions will not be considered for further evaluation. Concepts rated as possibly or questionable for many of the questions will be eliminated from further evaluation. Too many unknowns to a given concept will deter further considerations because of the short timeline of the project.

A Pugh chart is the final level of evaluation for a concept. Concepts will be evaluated using criterion that provide a quantitative measure of the concept's robustness. Criteria made for the Pugh chart are based on the requirements and specifications. Criteria were weighted quantitatively in comparison to one another to describe how important each criterion is. The greater the importance of a criterion, the greater the weight given. A quantitative scale of superiority and inferiority was given to each concept in relation to each criterion. A superior concept is scored with a higher number than an inferior concept. The weights of the criteria and concepts are then multiplied together to obtain a quantitative value that describes the robustness of a concept compared to all of the criteria.

Methods of Compression

Compression was the most complex subsystem, and subsequently had the largest solution space. This meant that relative to the other subsystem, concepts of a much broader breadth were generated. With the requirements and specifications in mind, a feasibility check was performed on all of the designs using the constraints shown in Table 4. This meant that given our general knowledge and previous experience on topics pertaining to the generated concepts, we evaluated whether each concept was likely generally practical and effective. The expanding foam and chemical reaction compression methods were subsequently removed from further evaluation methods. This is because expanding foam and chemical reaction would generate heat when providing the work that the piston will use to compress the cells. The cells need to remain within a degree Celsius of ambient to remain healthy; therefore, both ideas fail the constant temperature criterion. During actuation, we assumed that the amount of material reacting would vary; thus, the applied force would vary. A varying applied force is not repeatable nor is it precise. Lastly, as the compression needs to last for one hour, we thought it would be impossible for a reaction at that small of a scale to provide a force for that long.

The concepts of microfluidic compression and fluid pressure from a compression sleeve were ruled out during our consideration of technology readiness. Microfluidic compression would have involved advanced technologies that were non-trivial and difficult to create given our lack of experience and limited amount of time. Fluid pressure from a compression sleeve would have been difficult to manufacture in-house, as the sleeve would be at microscale and made with material that can expand with pressure. Furthermore, our team was not certain that the appropriate materials and manufacturing options exist to carry out this concept. It is possible that the manufacturing of the sleeve could be outsourced; however, this would add cost and time to our project that would cripple our chances of completing the project by our deadline.

The remaining compression actuator concepts were subjected to a Pugh chart, seen in Table 5. The criterion of the Pugh chart was developed considering constraints derived from the engineering requirements and specifications.

Table 5: Pugh Chart of Actuation Methods.

Pugh Chart For Actuators Within Piston/Cylinder						
Criterion:	Weight	Motor With Linkage	Solenoid	Magnet	Fluid Pressure	Spring
Size	2	-1	1	0	-1	1
Materials	1	1	1	1	-1	1
Ease of Assembly	2	0	1	-1	-1	-1
Compatibility With Multiple Actuations	2	1	0	-1	-1	-1
Manufacturability	3	1	1	1	0	1
Time Between Min and Max Compression	3	1	-1	-1	0	1
Reliability	3	1	1	1	1	1
Cyclic Ability	3	1	1	0	0	-1
	Totals:	**13**	**11**	**0**	**-4**	**5**

The Pugh chart narrowed down the actuation method to a motor with a linkage or a solenoid. A motor with linkage was chosen based on the Pugh chart. Several factors influenced this decision, one of which was a meeting with Grace where concerns about how quickly solenoids actuate were articulated. If the force were applied too quickly, the spheroids could be damaged. For a solenoid to actuate without damaging the spheroids, a dampener would have to be used. Our team was not certain of how a dampener could be coupled with a solenoid. Additionally, it would be difficult for a single solenoid to actuate the three separate rows of pistons, and possibly could require a linkage similar to the motor. Adding a solenoid for every row is likely not feasible given our size requirement of the design. The motor with linkage was evaluated as the better choice as it addresses most of the problems faced with the solenoid. Unlike a solenoid, a motor's speed is controllable, and its actuation is not binary (on/off). Linkages would have to be designed for both methods regardless; therefore, the motor with linkage was determined to be the most suitable actuation method for our final design.

Methods of Media Flow

The media flow orientations will be developed with the goal of creating a system that is conducive to media flow, so that media would alway circulate within the spheroid housings. It is difficult to determine which method creates the optimal flow without detailed analysis of the various scenarios presented in Figure 11. Vertical flow, while creative, has no advantages but has several disadvantages when compared to the other methods. This method likely limits the

amount of channels possible per container, and would require tubing between each container, which other designs would only need tubing between each row of containers. Designing tubes to flow through the piston is non-trivial; thus, requiring more time spent to design a workable solution.

Single-channel flow could be practical, seeing as the compartments are small. It is possible that the difference between one or two inlets per container would make a negligible difference. From a qualitative standpoint, however, it would seem that multi-channel flow would ensure that media would reach all corners of the container, with little extra time or monetary cost. Going into the development of the final design, we will compare the quantitative difference between single or multiple channels.

Additionally, pros and cons were developed with respect to series and parallel channels for each row. series channels would require less tubing as the bends at the end of each row would be smaller than the individual tubes required at the inlets/outlets of the rows in the individual channel design. This design would also be easier to manufacture, as splitting the inlet and outlet tubes from the media bag could be non-trivial. The parallel channels could be advantageous when considering the valves that will be necessary at the beginning and end of each row to facilitate each row's media flow rate. Ultimately, computer simulations of the fluid dynamics of each design will likely be the main factor in making a decision, and as of now neither method seems significantly better than the other. The computer simulations of each flow design's fluid dynamics are shown within the Media Flow Computational Analysis section of the report. The final decision between the two flow designs are discussed within the Final Design section of the report.

FINAL DESIGN

After the concept evaluation stage we then concentrated our focus on finalizing our device design. From concept evaluation, we first narrowed our focus on our method of actuation to using a motor and came up with a linkage that would allow our required strains. We then chose our materials, manufacturing process and developed a full CAD model using Solidworks.

Mechanical Subsystem

After gaining the additional requirements from our sponsor after DR2 we wanted a design that would allow both cyclic and static compression as well as the ability to control the rate of compression. With this in mind, a device actuated by a solenoid was thrown out due to the lack of control, so we shifted our focus to using a motor. We did this by designing a linkage where we will attach the motor directly to the crankshaft, and a push rod link will be attached to the pistons. With the torque analysis shown within the Engineering Analysis subsection of the report, we were able to source our motor and finalize the design. This specific linkage design allows the pistons to start at the same initial position then be in different final positions by rotating the

crankshaft 20 degrees. To ensure the fasteners do not come loose we are using nylock nuts with an option for blue threadlock if necessary. The model of our device can be seen below in Fig. 12.

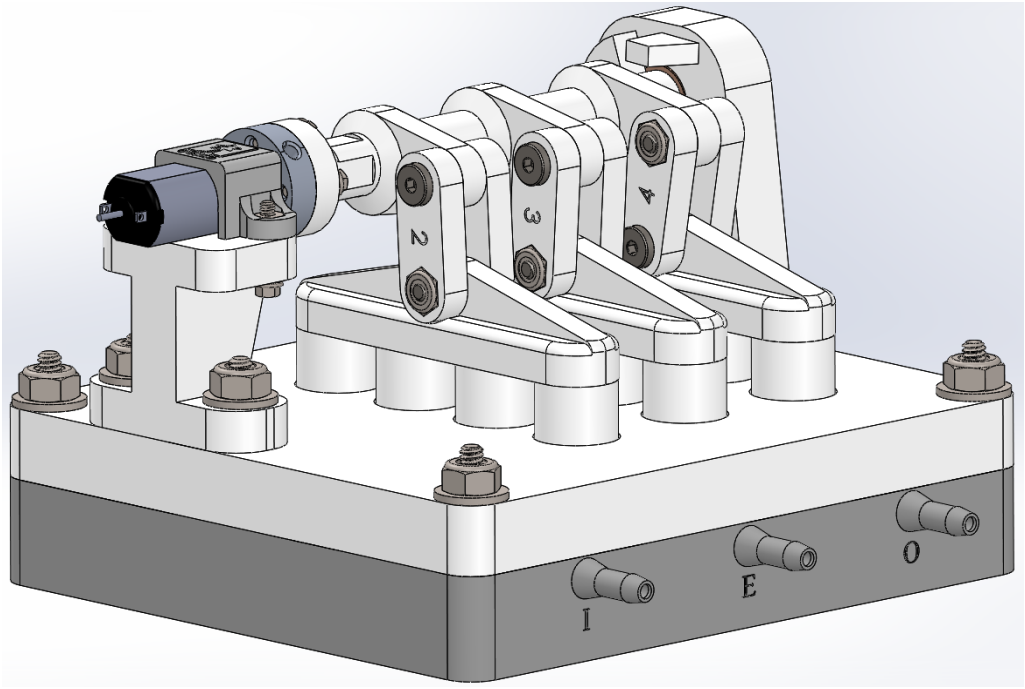

Figure 12: Shows the most recent Solidworks model to date.

To design such a linkage we created a sketch in Solidworks where we drew the initial position and final position on top of each other, as shown in Fig. 13. By setting constraints we could input how much rotation we wanted and the distance the piston has to travel. We then copied the same sketch two more times so we could change the distance traveled to get the stains we wanted. By adjusting some of the position constraints we could optimize the transmission angles. We were able to have a linkage where all the transmission angles fall within 15 degrees from 90.

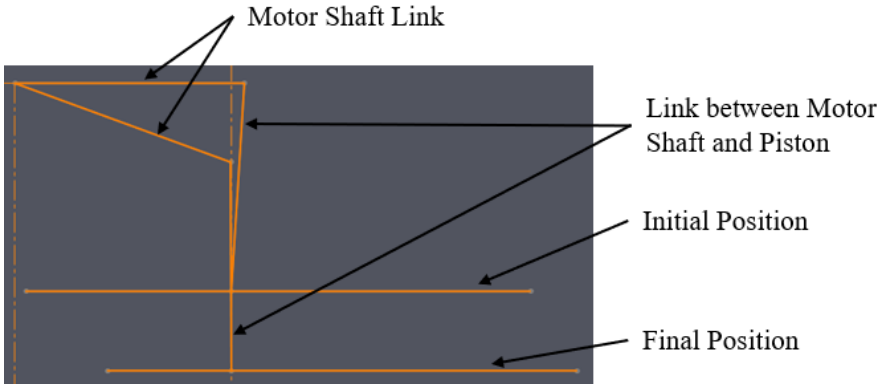

Figure 13: Shows the sketch for the 20% strain linkage with the initial and final position the linkage travels.

With the design of compression completed we tackled the problem of media flow. From our simulation work in COMSOL within the Engineering Analysis subsection of the report, we decided to use a series set-up where the media will follow one path through each of the cylinders through 1/8 inch internal tubing with another channel to allow the media to escape during compression. We are still working with Space Tango on the size of tubes they use and how they would attach but at this time we chose to print hose barbs onto the base where you can slip the tubes over them and use a hose clamp to ensure no leaks shown in Fig. 12 above. While the media is being flowed through our device we wanted to ensure none would leak out, so we found an o-ring on mcmaster that is designed for dynamic applications that we attached to each of the pistons and used a EPDM rubber gasket for the control set that sees no compression.

With the device currently being 4.5 by 4 inches we wanted the assembly to be easy once we hand it off to our sponsor. We designed the linkage to be attached to only the top piece where we plan to have it pre-assembled. This allows for a simple top-down assembly where one would only need to take off the four nuts in the corners and some tubing to have full access to the test specimens. The cylindrical extrusions mate coincidentally in the top piece self-centering itself and negate the need for a gasket between the two pieces as the piston only travels in the bottom piece except for the control group. Fig. 14 below illustrates the only assembly necessary once handed off to our sponsors.

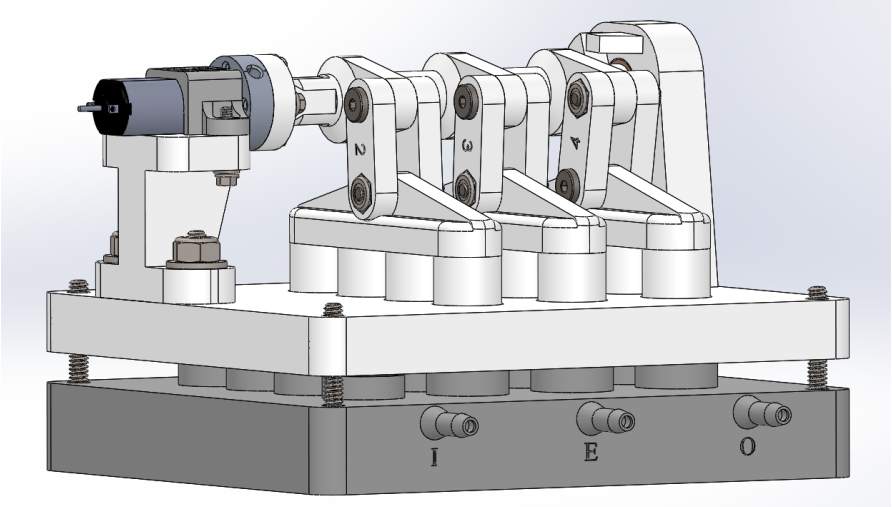

Figure 14: Shows how the linkage is only attached to the top piece allowing for ease of assembly.

Motor Choice

In order to actuate the pistons to compress the collagen gel, an actuator for our device is an imperative. Within the Methods of Compression section of the report, our team deduced that a motor with linkage actuator would most satisfy our requirements. Furthermore, the motor with

linkage actuator was displayed pictorially and its function explained within the Mechanical Subsystem section within the report.

The motor that our team chose was the Pololu: 380:1 Micro Metal Gearmotor HPCB 6V with Extended Motor Shaft. The motor specifications and dimensions are shown in Fig. 15 and 16 [11]. In terms of physical size this motor is an ideal choice, as a small motor is well suited for the physical size engineering specification for our device. This is evidenced by the fact that the motor length is 26 mm. From the Required Motor Torque Analysis section of the report, the total required torque from the motor is $7.66N \cdot mm$ ($0.078kg \cdot cm$). The Pololu motor has a stall torque of 5.0 $kg \cdot cm$ at 6V. In other words, the safety factor is 64.1, which proves that this motor can provide the necessary torque.

In order to control the movement of the motor during operation an Arduino Uno, H-bridge, and a motor encoder are used. Code in the proprietary Arduino language is uploaded to the Arduino via an external computer. To turn the motor on and off, the code instructs the Arduino to send a digital 5V signal to the H-bridge to determine whether or not to send power to the motor, as well as what direction to turn the motor in. The Arduino also uses a pulse width modulation signal to instruct the H-bridge as to how much power to send to the motor, which influences the speed it rotates at. Finally, the encoder mounted to the motor precisely measures its position and feeds it back to the Arduino for accurate control of motor position.

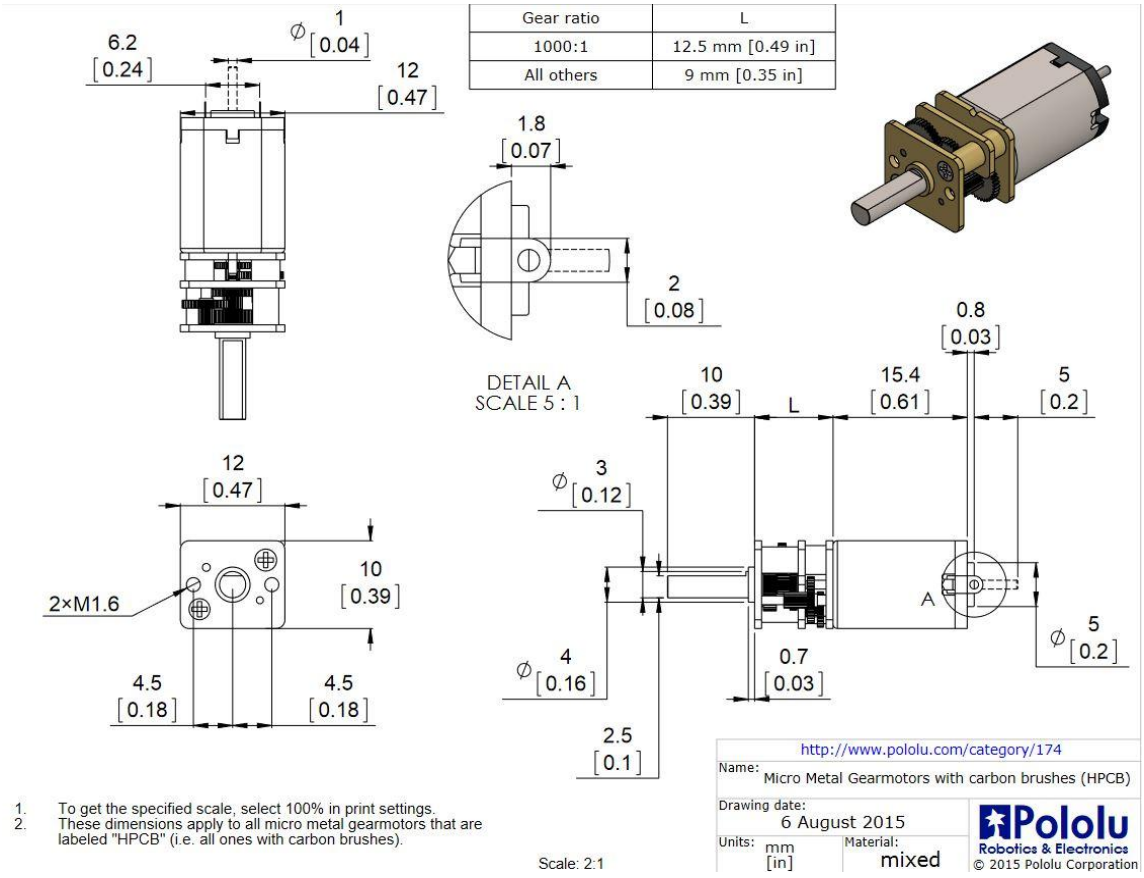

Figure 15: Pololu motor engineering drawing [11].

Dimensions

Size:	10 × 12 × 26 mm[1]
Weight:	9.5 g
Shaft diameter:	3 mm[2]

General specifications

Gear ratio:	379.17:1
No-load speed @ 6V:	85 rpm
No-load current @ 6V:	0.10 A
Stall current @ 6V:	1.5 A
Stall torque @ 6V:	5.0 kg·cm
Max output power @ 6V:	1.1 W
Extended motor shaft?:	Y
Long-life carbon brushes?:	Y
Motor type:	1.5A stall @ 6V (HPCB 6V - carbon brush)

Performance at maximum efficiency

Max efficiency @ 6V:	30 %
Speed at max efficiency:	68 rpm
Torque at max efficiency:	1.0 kg·cm
Current at max efficiency:	0.40 A
Output power at max efficiency:	0.71 W

Notes:

1 Output shafts add 14 mm to the 26 mm length.
2 D shaft.

Figure 16: Pololu motor dimensions, general specifications, and performance at maximum efficiency [11].

Material Choice

Our device material must be impermeable to media, manufactured with high resolution, and withstand any stresses that may occur during assembly and or testing. Thus, our team decided to use Formlabs Standard Green Resin. The green resin used for our device is manufactured by running a Formlabs Form 3 3-D printer. A Form 3 3-D printer and green resin is provided free of charge by Liu Lab, which reduces the cost of our device when compared to other material choices. The Form 3 has a build volume of 5.7 x 5.7 x 6.9 in, which is smaller than the build size of any of our device components; thus, our components can be built within the Form 3. From Solidworks, the estimated amount of green resin used for our device is 399.28 g. However, this does not include the weight of the motor, fasteners, tubing, and valves that will be used in our device. As weight is not a concern for our sponsor, and as such our team as well, this approximate resin weight is reasonable for our purposes. A photo of the Form 3 is shown in Fig. 17 [12].

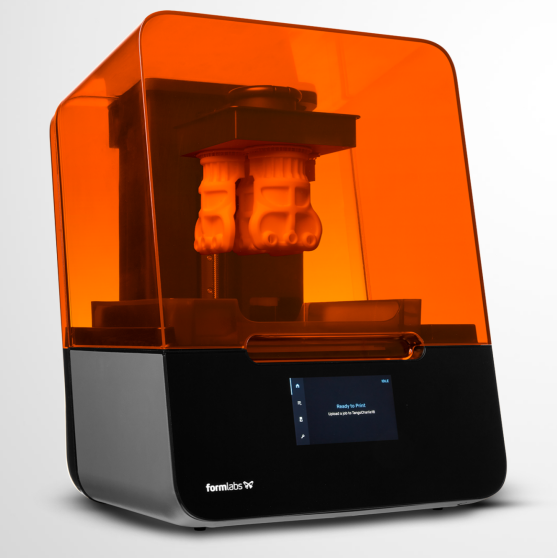

Figure 17: Formlabs Form 3 3-D Printer. [12]

The Form 3 can provide a 3-D printed layer thickness of 100 μm when using the green resin. When the layer thickness is 100 μm, the green resin has an ultimate tensile strength of 38 MPa, a tensile modulus of 1.6 GPa, a flexural modulus of 1.25 GPa, an elongation at failure of 12%, and a heat deflection temperature lower bound of 42.7 ℃ at 1.82 MPa [13]. Given that the testing environment on the ISS is at a temperature of 33.5 ℃, and the testing will not result in component stresses anywhere near 1.82 MPa, our device will not deform from heat deflection. As shown in the Collagen Gel Compression Analysis section of the report, the total required force required to strain the collagen gel is 0.3 N. Given the material properties of green resin, the maximum force required from testing is 0.3 N, and the physical size of the design components, it is extremely unlikely that any design component will fail under load. The Linkage Arm Stress Analysis section of the report supports this claim. The analysis shows that given our current

material the linkage arms and cylinder walls will not fail, nor deform under our current loading regime.

Media Flow Channel Subsystem

As was discussed within the Concept Evaluation section of the report, two preliminary media flow channel designs had passed concept evaluation. It was concluded that our team had to conduct computational analysis on each of the two designs to determine which design was most conducive to media flow. An in depth explanation of the assumptions, methods, and results of the computational analysis conducted is within the Engineering Analysis section of the report.

A schematic of the series and parallel media flow designs are shown in Fig. 18. Both designs are symmetrical, which means that the inlet and outlet valves may be placed on either external hole. Both designs have channeling that is internally routed within the base of our device, reducing the amount external tubing necessary to flow media. For the series design, the media flows through all of the cylinders in order from inlet to outlet. For the parallel design, media flow is split between four separate channels in series through an inlet manifold and then flow congregates through an outlet manifold. The escape channeling for the media was not included within the analysis for computational simplicity. A further explanation of the escape channeling will be discussed within the Media Flow Escape Channel section of the report. The following results that compare media flow characteristics between the series and parallel designs are from COMSOL computational analysis, as shown in Tables 6 and 7.

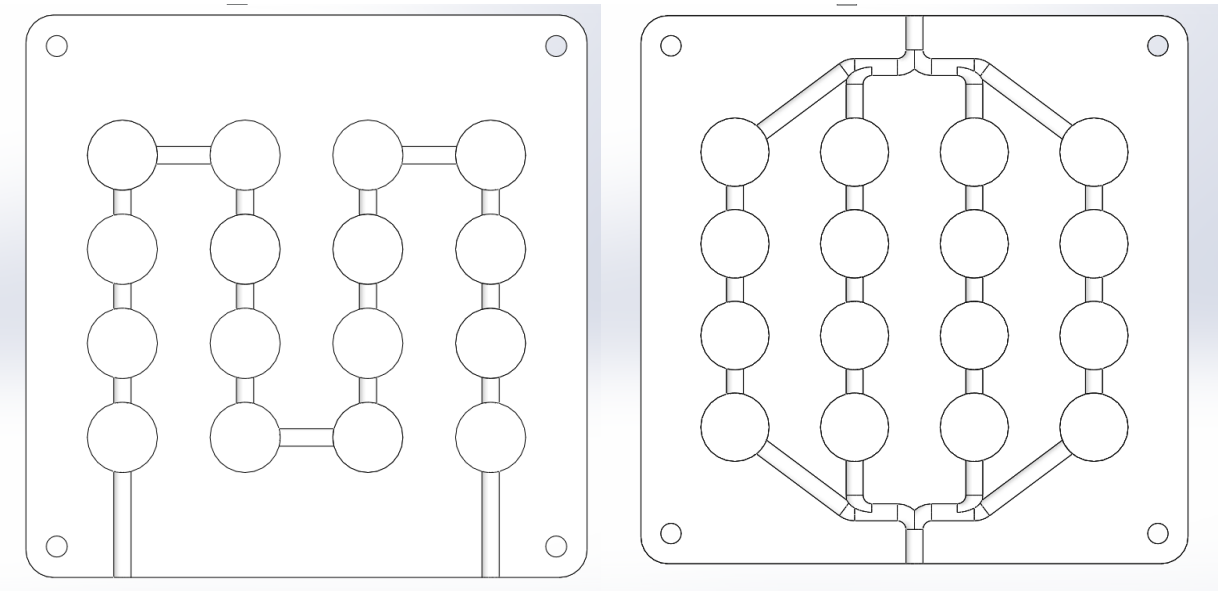

Figure 18: Schematic of series (left figure) and parallel (right figure) media flow designs.

Table 6: COMSOL analysis results of the series media flow designs.

Maximum Media Velocity (mm/s)	Media Velocity Within Cylinder (mm/s)	Pressure Gradient (Pa)
14.1	5 - 6	3.11

Table 7: COMSOL analysis results of the parallel media flow designs.

Maximum Media Velocity (mm/s)	Media Velocity Within Cylinder (mm/s)	Pressure Gradient (Pa)
13.8	3 - 4	0.70

Based on the results from the COMSOL computational analysis, the series flow design was more conducive to media flow than the parallel flow design. A higher flow velocity and pressure gradient implies that the design is more conducive to media flow, and vice versa. The maximum flow velocity of the series design was 0.3 mm/s more than the parallel design. In the best case scenario for the parallel design, the series design had a flow velocity within the cylinder that was between 1 to 3 mm/s more than the parallel design. The pressure gradient for the series design was 2.41 Pa more than the parallel design.

For the parallel media flow design, the discrepancy of media velocity between the sets of cylinders is due to the imperfections of the inlet and outlet manifold geometry. The imperfections of the manifold geometry cause flow to be channeled in a non-equitable manner between the sets of cylinders. When flow channeling is non-equitable, the flow characteristics of the media will differ between the sets of cylinders. Furthermore, the pressure gradient between the sets of cylinders varies. The media pressure gradient is lower on average for the outside set of cylinders than the inside set of cylinders.

When the media flow characteristics and channeling are non-equitable between the sets of cylinders, the cells within the collagen gel will receive varying amounts of media. As media nourishes the cells before compression testing, it is imperative that cells receive equal amounts of nourishment. This is because compression testing is to be performed on nourished cells, and if testing is done on under-nourished cells along with nourished cells, the results of the experiment may be void due to non-controlled variability between the sets of cells.

With this being said, it is possible to alter the inlet and outlet manifold geometry to allow for equitable media flow between the sets of cylinders. The redesign of the manifold would require our team to spend additional time on CAD, COMSOL, and research into manifold technologies. This in of itself is not an issue, but late into our design process any additional time placed into R&D of a design is more costly than an early stage R&D of a design. In our case, this is due to the time constraints placed on our project. Resources would have to be placed into the design of the manifold which would have otherwise been allocated to other project needs. It may happen that a parallel flow design with a revised manifold geometry may be more conducive to media

flow than our current series flow design; however, the actual costs of figuring out if this claim is true outweighs the supposed benefits of a revised manifold geometry. Thus, our team decided to include the series flow design over the parallel flow design in our final device design.

Media Flow Escape Channel

To solve the engineering specification that media must partially vacate the cylinders to avoid a media pressure build up during compression, our team used CAD to create a design for a media flow escape channel. As media is an incompressible fluid and gel is permissible to media, our team does not want media within the cylinders at the time of gel compression. Our escape channeling will be a cavity within the base of our device. Our design is shown in Fig. 19.

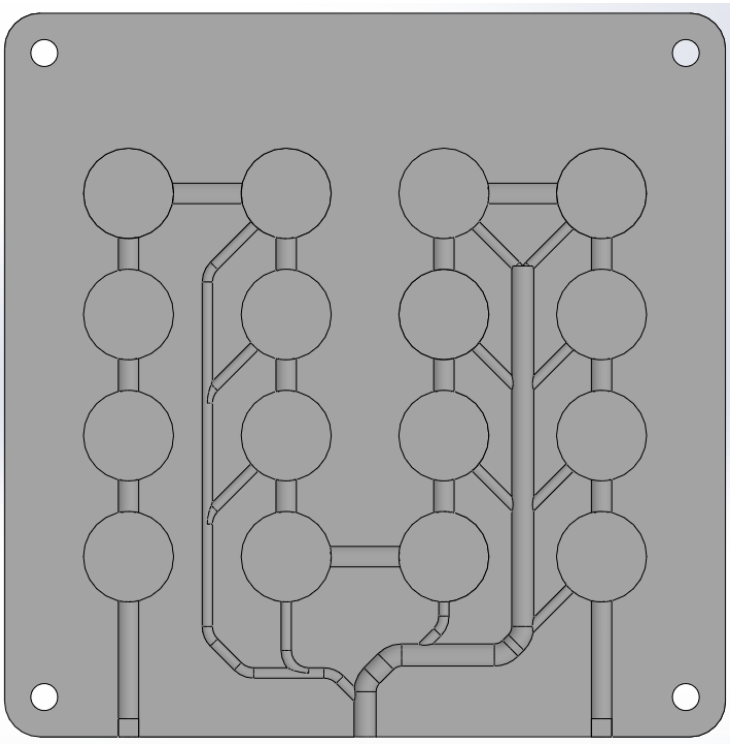

Figure 19: Preliminary media flow escape channel design.

ENGINEERING ANALYSIS

In order for our final design to satisfy the engineering specifications, our team conducted computational, and hand-written calculations as evidence that our design does indeed meet the specifications. Analysis on media flow within flow channels, stress tests on the linkage arms and cylinder walls, required force to strain the collagen gel, and required motor torque are shown below.

Media Flow Computational Analysis

The media flow in our system is essential because the cells receive media nutrients so that they are nourished during compression testing. Thus, it is important to understand the steady state flow properties of our design's channeling. As stated in a previous subsection of this report, Methods of Media Flow, our team at the end of our concept evaluation phase of our project was unsure of what final media flow orientation design to go with. Furthermore, we stated that computational analysis was necessary to decide between the two orientations, series and parallel.

In our system, media would be pressurized from a reservoir to our design via a pump provided by Space Tango. Media would enter and exit our design through inlet and outlet valves. Thus, the volumetric flow rate and pressure of the media entering and exiting our system can be controlled through the type of pump and valves used in the system.

To further understand our two flow channel designs, COMSOL computational modeling software was used. The following modeling was done in the aim to find which design was more conducive to media flow. The boundary conditions used during modeling were a volumetric flow rate of media being 3.2 ml/min, and an assumed pressure of 1000 Pa of the media from the pump. We assumed that the pump was 1000 Pa as a reasonable estimate to what an actual pump of this size would provide to pressurize fluid. Whereas the volumetric flow rate of the media came from our engineering specifications. All internal pipes have a diameter of ⅛" and all cylinders have a diameter of ¼". The walls that make up the pipes and cylinders were assumed to have no porosity nor permeability to media. Both series and parallel flow designs have these boundary conditions.

As media will be flowing through pipes and cylinders with gel in them, the gel's porosity and permeability constants were used to model media flowing into the gel to nourish the cells. Based on a *Scientific Reports* article published in 2019, three researchers of the University of Leipzig found that the average porosity of collagen gel, which is approximately the same gel that will be within our device, had an average porosity between 0.95 and 0.98 [14]. Thus, our team decided to model the gel with a porosity of 0.965, directly in the middle of the reported porosity average of collagen gel. Based on a *ScienceDirect* article published in 2013, four researchers from McGill University found that in their research that the collagen gel microstructure has a permeability between 10^{-15} and 10^{-14} m^2 [15]. Thus, our team decided to model the gel with a permeability of $5 \times 10^{-15} m^2$, directly in the middle of the reported permeability average of collagen gel. Both series and parallel flow design had these gel parameters modeled in.

Series media flow design COMSOL results

For the media velocity within the series flow design, as shown in Fig. 20, the maximum media velocity is 14.1 mm/s and the minimum velocity is 0 mm/s. The minimum velocity is 0 mm/s because when the media flows into the gel, due to the gel porosity and permeability to media, the

media within the gel is modeled to not flow at point thereafter; thus, the velocity of the media is 0mm/s within the gel. The media within the cylinder on the same flow path as the piping has a velocity anywhere from 5 to 6 mm/s.

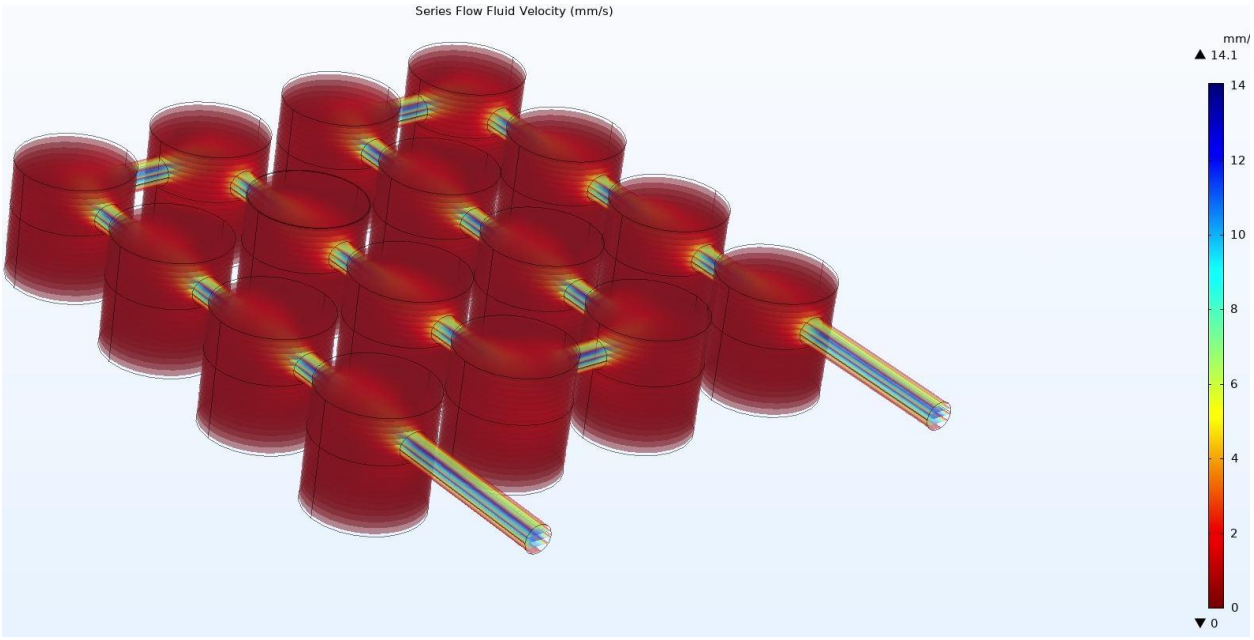

Figure 20: Media flow velocity of the series media flow channel design. Inlet of the media flow is the left valve and outlet of the media flow is the right valve.

For the media pressure gradient within the series flow design, as shown in Fig. 21, the maximum pressure is 1000 Pa at the inlet boundary and the minimum pressure is 996.89 Pa at the outlet boundary. The pressure gradient is 3.11 Pa per 1000 Pa.

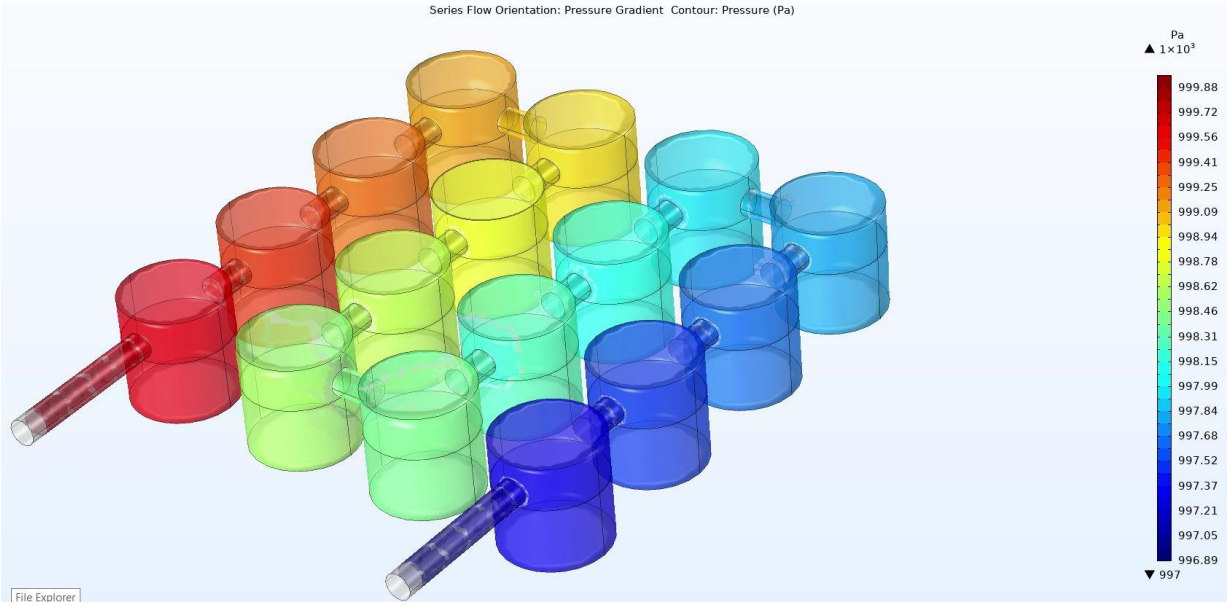

Figure 21: Media flow pressure gradient of the series media flow channel design. Inlet of the media flow is the left valve and outlet of the media flow is the right valve.

Parallel media flow design COMSOL results

For the media velocity within the parallel flow design, as shown in Fig. 22, the maximum media velocity is 13.8 mm/s and the minimum velocity is 0 mm/s. The minimum velocity is 0 mm/s because when the media flows into the gel, due to the gel porosity and permeability to media, the media within the gel is modeled to not flow at point thereafter; thus, the velocity of the media is 0mm/s within the gel. The media within the cylinder on the same flow path as the piping has a velocity anywhere from 2 to 4 mm/s. The velocity of the media varies within each set of four cylinders. The velocity of the media on the outside set of cylinders is anywhere from 2 to 3 mm/s and on the inside set of cylinders is anywhere from 3 to 4 mm/s. The discrepancy of media velocity between the sets of cylinders is due to the imperfections of the inlet and outlet manifold geometry. The imperfections of the manifold geometry cause flow to be channeled in a non-equitable manner between the sets of cylinders.

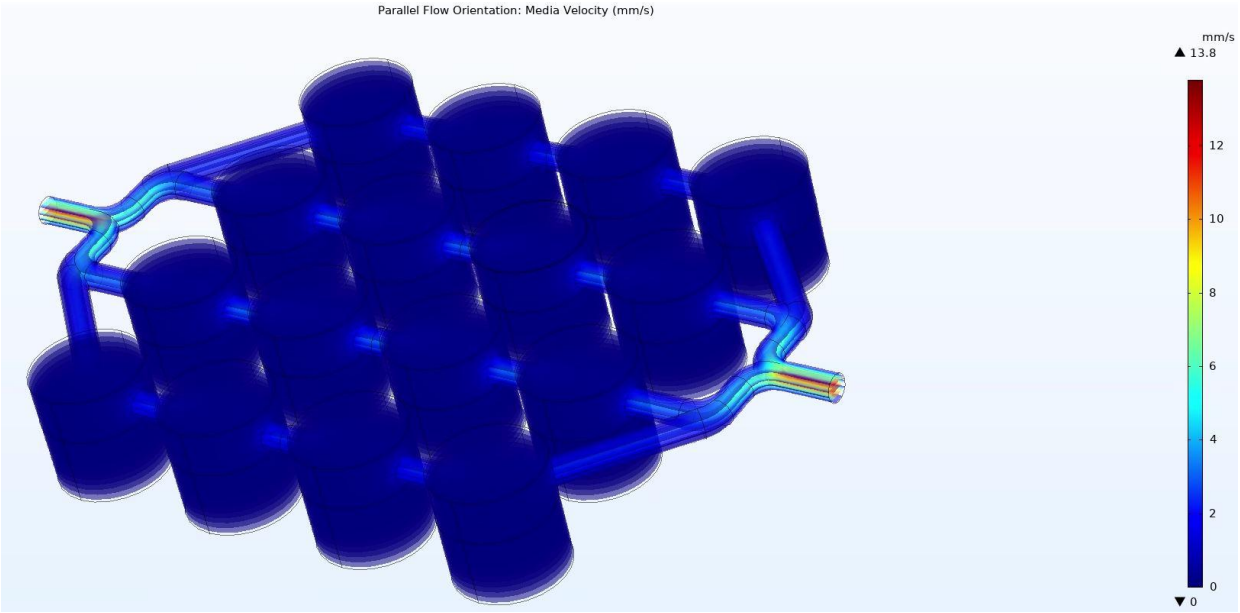

Figure 22: Media flow velocity of the parallel media flow channel design. Inlet of the media flow is the left valve and outlet of the media flow is the right valve.

For the media pressure gradient within the parallel flow design, as shown in Fig. 23, the maximum pressure is 1000 Pa at the inlet boundary and the minimum pressure is 999.30 Pa at the outlet boundary. The pressure gradient is 0.7 Pa per 1000 Pa. The media pressure gradient is lower on average for the outside set of cylinders than the inside set of cylinders. The discrepancy of media pressure gradient between the sets of cylinders is due to the imperfections of the inlet and outlet manifold geometry. The imperfections of the manifold geometry cause flow to be channeled in a non-equitable manner between the sets of cylinders.

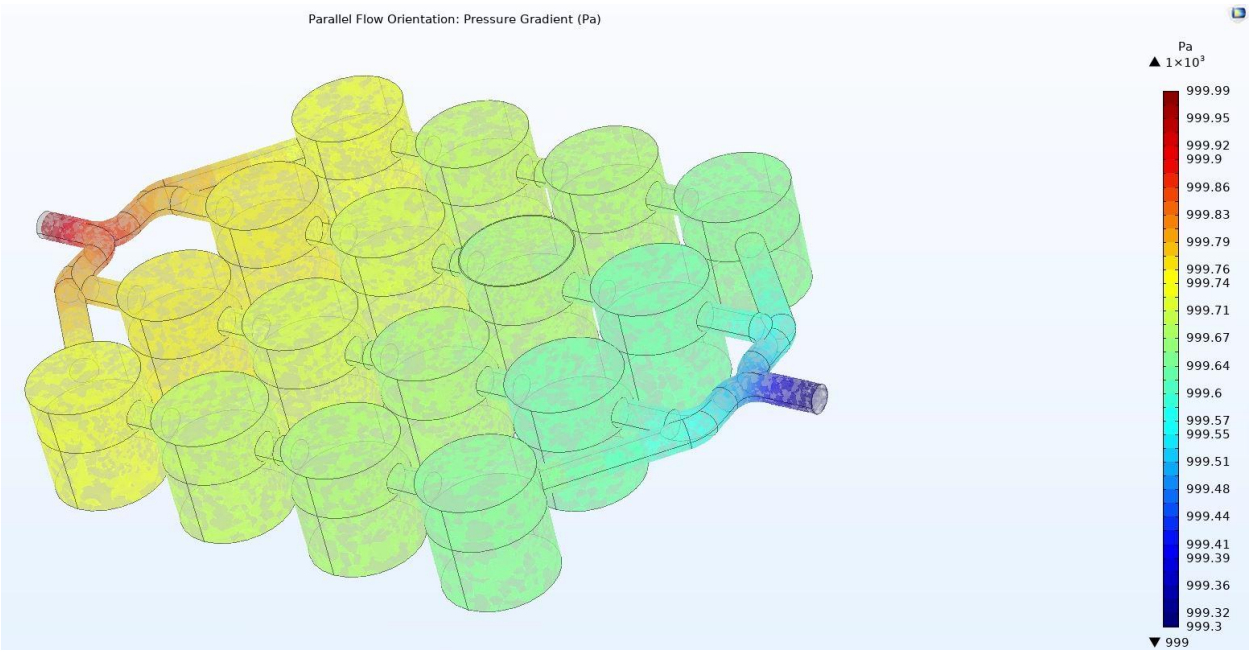

Figure 23: Media flow pressure gradient of the parallel media flow channel design. Inlet of the media flow is the left valve and outlet of the media flow is the right valve.

Collagen Gel Compression Analysis

In order to find the required torque through the shaft, it is necessary to find the force required to strain the collagen gel. The required volumetric strains on the gel are 10, 20, and 30%. As the gel is within a fixed cylinder, the strain only acts in one dimension. The fixed cylinder diameter is 0.0127 m. As such, we assumed uni-axial strain within the linear elastic deformation regime for our calculations. This is a safe assumption for our design, as the strain will be generated by a piston compressing the gel by a set distance. Even if the assumption of linear elastic deformation has error when compared to reality, our team can apply a safety factor to any component when using this force in calculations. There will be a set of four pistons that provide a 10% strain, a set of four pistons that provide a 20% strain, and a set of four pistons that provide a 30% strain to the gel within each cylinder.

Our sponsor stated that the Young's modulus of collagen gel is 1000 Pa. Furthermore, from a published article from 2016 in the *Journal of Materials Science: Materials in Medicine*, six researchers from the University of Sheffield state that the Young's Modulus of collagen gel from their research is 1000 Pa [16]. This value of Young's Modulus is subject to change because our sponsor may make the concentration of the collagen gel higher by infusing the gel with a polymer.

From using the known cylinder diameter, strain, and Young's modulus of the gel, we can find the required force needed to strain the gel by the prescribed amounts using Eq. 1:

$$E = \frac{\sigma}{\varepsilon} = \frac{F}{A} \div \varepsilon \quad (1)[17]$$

where E is the Young's modulus of the gel, A is the force contact area of the gel, ε is the strain and F is the required force per cylinder. When Eq. 1 is rearranged to solve for the required force and multiplied by four to account for the set of four cylinders, the following results ensue, as shown in Table 8.

Table 8: Required force for each set of cylinders based on the prescribed strain.

Prescribed Strain	Required Force (N)
0.10	0.0501
0.20	0.1010
0.30	0.1520

Upon knowing these required forces, force, torque, and stress analyses of other subsystems on our design can ensue.

Linkage Arm Stress Analysis

Now that an estimate of the required forces are known, the stress within the linkage arms can be calculated. A linkage arm is between the design with the set of four pistons and the cam on the rotating shaft. Our analysis assumed the linkage arm to be a two force member, as shown in Eq. 1:

$$\sigma_{internal} = \frac{F_{cyl}}{A} = \frac{F_{cyl}}{w \times d} \quad (1)[18]$$

where F_{cyl} is the required force to strain the gel by 30% within one cylinder, A is the cross sectional area of the linkage arm, w is width of the linkage arm, d is the depth of the linkage arm, and $\sigma_{internal}$ is the internal stress that a linkage arm experiences from the resultant forces from straining the gel. As there are two linkage arms, the internal stress was assumed to be divided evenly between the two linkage arms. Thus, as every term in the analysis was known except for the internal stress, the internal stress can be solved for. The result is shown below.

$$\sigma_{internal} = 168.45 \text{ Pa}$$

As is shown in the Material Choice section of the report, the material used for linkage arms has an ultimate tensile strength of 38 MPa. The internal stresses within the linkage arms are about 200,000 times smaller than the ultimate tensile strength. As such, the linkage arms are appropriate for our purposes.

Required Motor Torque Analysis

In order to source a motor, a torque analysis on the shaft was performed. There were two forces that propagated to create a torque on the shaft. First, there was the force that the gel exerted on the piston, and secondly there was the friction between the O-ring and the sides of the piston. Using these forces, a statics analysis was performed to find the moment on the shaft.
The force that the gel exerts on the piston was determined previously on Collagen Gel Compression Analysis section of the report. Using this force, a torque analysis was performed to find the moment of each strain condition on the shaft. A detailed example of this analysis is shown in Appendix (A.1).

For the second analysis regarding the torque created by the friction of the O-ring and the cylinder walls, the force of friction was calculated. An estimate of the coefficient of friction for plastic on rubber was found to be 0.7 [19]. The normal force was calculated by Eq. 1, considering the strain of the O-ring and its Young's modulus, both of which were known.

$$E = \frac{\sigma}{\varepsilon} = \frac{F}{A} \div \varepsilon \quad (1)[17]$$

After determining this, the torque was calculated in the same way as the first method. The results of this analysis can be seen in Table 7.

Table 9: Required torque for each row of cylinders based on the prescribed strain.

Prescribed Strain	Required Torque (N·mm)
0.10	1.37
0.20	2.47
0.30	3.82
TOTAL	**7.66**

In knowing the required torque, the motor used for the final design can be selected based on the motor's torque specifications, which is discussed within the Motor Choice section of the report.

DESIGN RISK ASSESSMENT

Our design is controlled and surrounded by electrical components, regardless if the testing is done on Earth or the ISS. As such, the device was designed and analyzed not only in regards to collagen gel stain application and media flow conduciveness, but also for tester and ISS safety. On Earth, media is subjected to gravitational forces that keep media from floating when free of any container. On the ISS, media is subjected to micro-gravitational forces that do not keep media from floating when free of any container. As such, our team assumes that a leak could cause more damage within a micro-gravity situation within a tight container, such as the CubeLab on the ISS. Additionally, a failure of the motor during testing could cause the

experiment to fail. The following paragraphs will describe the risks associated with media leakage and motor failure.

One of the factors that can prove unsafe to testers and to the ISS is leakage of the media into the experiment setup area or CubeLab. This is because in both situations, the device will be powered and surrounded by electronic components. If electronic components come into contact with media, the possibility of an electrical short is high. An electrical short would generate an excess of voltage and cause excessive flow of current in the power source. An electrical short can destroy electrical components in connection with the shorted component. Furthermore, an electrical short is a fire hazard because the excess flow of current can generate a lot of heat, which can cause components to catch fire or ignite combustible substances. The final iteration of the device going to the ISS may very well be connected to electrical components that are protected by circuit breakers; however, even though a circuit breaker may reduce the fire hazard of an electrical short, the circuit breaker will not prevent damage of the components from direct contact with the media. Additionally, if a leakage were to happen the experiment would be a failure, which would cause major setbacks to our sponsor's experimental goals.

With all of that said, it is good design practice to design the device to reduce the possibility of common modes of failure. Thus, the device was designed to prevent leakage of media through the use of o-rings on the piston walls and barbs at the device flow entrances. When the piston walls are within the cylinder cavity, the o-ring will make contact with the cylinder walls; thus, creating a leak tight seal that holds the media within the device channeling during dynamic and static scenarios. To achieve this seal, a 0.504 inch diameter rubber o-ring was attached to the piston that causes an interference fit of 0.004 inches between the o-ring and cylinder wall. When flexible tubing is connected to the barb, the inner diameter of the tube will tightly fit about the outer diameter of the barb; thus, creating a leak tight seal. To achieve this seal, an eighth inch inner diameter PVC plastic tube is attached to the barb, which causes a diameter interference fit of 0.04 inches. The amount of interference between the tube and barb along with the tube material allows for a tight seal without a hose clamp. The two design features have mitigated the safety concerns from media leakage to an acceptable level.

A further risk of failure of the device is a motor failure. A motor failure can indirectly cause damage to the surrounding device environment and directly affects the cells within the collagen gel. An indirect risk of a motor failure is if the motor rotates in the opposite direction beyond the zero point. Rotating the motor too much in the opposite direction can cause media leakage due to the o-rings being above the cylinder walls. The direct risk of a motor failure is if the motor rotates in the correct direction beyond the specified 20 degrees of rotation. A rotation beyond 20 degrees can over strain the cells, which would result in a failed experiment. Another direct risk of a motor failure is if the motor does not actuate at all, resulting in an experimental failure due to a lack of strain on the cells. To try this experiment again in the future requires additional test

runs on Earth and the ISS, which statistically increases the likelihood of other modes of failure to occur. An additional risk due to motor failure is a device component catastrophically failing due to overloading. A failed component could become a projectile, which could injure a tester or damage surrounding components within the CubeLab. A risk assessment was conducted to determine the level of danger that a media leakage and a motor failure poses to our device, as shown in Table 10.

Table 10: Risk assessment of final device.

Hazard	Hazardous Situations	Likelihood	Impact	Technical Performance	Schedule	Cost (Based on BOM)	Action to minimize hazard
Media Leak	When using the device, the user and or surrounding electronics could be doused with the media	Medium	Serious	Significant degradation in technical performance or major shortfall in supportability; may jeopardize program success	Program critical path affected	Budget increase or unit cost increase. Budget > 5%	Ensure sealing components are situated properly in their designated positions, as shown in the assembly instructions
Motor Failure	When using the device, the motor could overly rotate, resulting in possible media leakage or physical damage	Low	Serious	Significant degradation in technical performance or major shortfall in supportability; may jeopardize program success	Program critical path affected	Minimal or no impact	Ensure the motor is tested before launch to ISS to validate functionality. Ensure motor wiring is secure and properly situated

DESIGN PROTOTYPE VALIDATION

The device was validated through physical testing. Due to the turnaround time of the 3D printer and resin supply limitations, a completed, functional prototype was unable to be validated in its entirety. However, the first prototype was able to be tested to determine if key benchmarks could be met in the future by a completed prototype.

The most important requirement of the device was to actuate the pistons via an Arduino controlled motor. Due to tolerance issues regarding the resin and its expansion, the prototype was not printed to specifications. Therefore, in order to prove that the pistons could actuate, the device was altered by sanding and dremelling it down to dimensions that facilitated actuation. With further trial and error of the dimensions of the pistons and spheroid wells, the motor would be able to successfully drive all three rows of pistons. Due to the issues with 3D printing and the

tolerances, fluid flow validation was limited to very basic testing. The channels of the device were printed to specifications, but without a prototype where all of the pistons could actuate, the escape channels could not be tested besides having a fluid (water) run through the device in the intended way, which was successful. In the future when a device with acceptable tolerances is manufactured, the pressure exerted by the pistons and a thorough fluid flow analysis could be conducted.

The prototype was also used to validate the functionality of the electronic components; namely, the Arduino, H-bridge, motor, battery, and their appendages. The integration of these components proved to be mostly successful. Physically, the electronic components were small enough to be packaged in a compact environment, and the motor was able to move the pistons. This motion was repeatable, and could be successfully controlled using the Arduino with code that we wrote. From a software and hardware perspective, we were able to demonstrate that the motor can operate cyclically as well as actuate just once. The main drawback from validating the electrical components was that the encoder was not successfully integrated into the system. While the motor is able to actuate properly, adding the encoder would make it much more accurate and will help the system meet the tolerances for pressure desired by the Liu Lab.

DISCUSSION OF DESIGN AND LESSONS LEARNED

Throughout the design process our team has learned a great deal about the final design presented in this report. As such, the true strengths and weaknesses that exist within this design have been realized by our team. These design attributes allow for potential improvements to be made through actionable and appropriate recommendations to the sponsors.

As with any design process that engineers go through, one gets the sense of how to be realistic in one's project ambitions versus the limitations that reality impose on projects. In this case, the limitations imposed on our project ambitions were deadlines, remote work, and other school work. The team's ambitions of the project were in accordance with the limitations of reality at the outset of this project. I think this is due to a couple of factors: first, the structure of the senior design course gave our team a great structure to abide by so that deadlines could be met; and second, our team prior to this course have been in two other design courses, which implicitly teach students not to be overly ambitious. As experience is a teacher, our team learned better how to apply this principle through the extra experience gained in this course. This principle kept the final design simple, cost effective, and functional. Another lesson our team learned was that a given manufacturer's tolerances on a part can be incorrect, as the tolerance specifications given on the Formlab website for 3D printing were incorrect for our prototype. This will be discussed further in a subsequent paragraph.

With our current design as well as previous interactions there are always strengths and weaknesses. One of the stronger features of our design is the fact that the linkage and the motor attaches to only the top piece. This means that the linkage can remain assembled and the user will only have to undo four nuts to have access to the test specimens. Another strength of our design in that only one motor is needed to operate the linkage. This allows us to optimize the overall size of the device and will ease the development of the motor's software. An advantage that pertains to the media flow function of our device is that we utilized internal tubing cutting down the need for more tubing and added barbs where the user can simply slide a hose over. Lastly, our device only requires three tools for the overall assembly and once the linkage is assembled only one tool is required. This simplifies the assembly and cuts down on the time for assembly.

One of the major weaknesses of our design is the fact that all our parts were designed to be manufactured with a 3D printer. While this is an advantage in a lot of aspects, our design requires a certain level of precision for the parts to fit and when building our prototype we found all the holes were printed a lot smaller than to what was specified. To mitigate this for still using a printer, we opened up tolerances and made most of the fits have a larger gap. If this is still a problem we recommend milling or drilling out some of the holes with either an endmill, drill, or reamer. This also leads us to the fact that most of our parts would be very hard if not impossible to manufacture in more traditional ways, mainly because of our internal tubing. If the device is to be milled we would recommend redesigning the tubing as to be able to flow media with external tubes and redesign the motor shaft where the links can be removed for ease of manufacturing. Another disadvantage of our design is the links are set for only a certain percentage of strain and can not be changed. If different strains were wanted you would need to print new links and a whole new motor shaft. We would recommend making each link adjustable with slots or multiple holes.

ENGINEERING STANDARDS

Research into the database of ASTM and ABET engineering standards yielded no relevant results regarding microfluidics nor the current project. As such, our team did not use any ASTM or ABET engineering standards throughout the project.

PROJECT BUDGET AND BILL OF MATERIALS

The overall budget for the project is $1000. We received this funding from the Liu Lab at the University of Michigan in order to design, build, and validate a solution for the previously stated stakeholders. To track our spending and ensure that this budget is not exceeded, the team has created a bill of materials that records the money needed to build our design, as shown in Table 9. The total cost of the design is $457.13, so there will not be any issue with exceeding the budget. This total is for the price of two devices and accounts for the cost of the resin that was

available in house.. The team tracked any other expenditures that occur, such as money used to buy materials for prototyping or parts used for testing. In all, our team has spent $351.59 excluding the cost of resin that we did not purchase. If needed, money can be saved through the use of more extensive simulation taking the place of tangible prototypes for empirical testing. Funding could also be conserved by sourcing cheaper parts and materials for the solution and any prototypes.

Table 11: Bill of Materials for our design.

Part Number	Part Description	Quantity	Material	Procurement Process	Total Price*	Parts Per Package	Manufacturing Plan
100	Base	2	Clear Resin	Liu Lab	$47.68	N/A	3D Printing
101	Cylinder Housing	2	Clear Resin	Liu Lab	$29.80	N/A	3D Printing
102	Piston	6	Clear Resin	Liu Lab	$17.88	N/A	3D Printing
103	O-ring	24	Buna-N Rubber	Purchase	$8.47	100	N/A
104	Motor Shaft	2	Clear Resin	Liu Lab	$2.98	N/A	3D Printing
105	Pillow Block motor	2	Clear Resin	Liu Lab	$2.62	N/A	3D Printing
106	Pillow Block	2	Clear Resin	Liu Lab	$2.96	N/A	3D Printing
107001	10% Strain Push Rod	4	Clear Resin	Liu Lab	$0.54	N/A	3D Printing
107002	20% Strain Push Rod	4	Clear Resin	Liu Lab	$0.54	N/A	3D Printing
107003	30% Strain Push Rod	4	Clear Resin	Liu Lab	$0.54	N/A	3D Printing
108	6-32 1.25" Bolt	8	8-18 SS Steel	Purchase	$6.33	25	N/A
109	6-32 0.75" Bolt	6	8-18 SS Steel	Purchase	$6.32	50	N/A
110	6-32 Nylock Nut	14	8-18 SS Steel	Purchase	$4.30	100	N/A
111	#6 Washer	14	8-18 SS Steel	Purchase	$8.22	25	N/A
112	4-40 Nylock Nut	12	8-18 SS Steel	Purchase	$5.16	50	N/A

113	Alloy Steel Shoulder Screw	12	Alloy Steel	Purchase	$21.60	10	N/A
114	3/8" Sleeve Bearing	2	Oil-Embedded Bronze	Purchase	$1.30	1	N/A
115	1/8" Tubing 5'	1	PVC Plastic	Purchase	$28.10	1	N/A
116	Hose Clamp	6	301 SS Steel	Purchase	$6.26	10	N/A
117	Gasket	8	EPDM Rubber	Purchase	$39.36	1	N/A
118	Motor	2	Various	Purchase	$37.90	1	N/A
119	Encoder	2	Various	Purchase	$15.90	1	N/A
120	Motor Controller	2	Various	Purchase	$13.78	1	N/A
121	Battery Plug	2	Various	Purchase	$5.99	8	N/A
122	Jumper Wires	1	Various	Purchase	$7.49	120	N/A
123	Arduino	2	Various	Purchase	$43.98	1	N/A
124	3mm Motor Hub	2	Aluminum	Purchase	$5.95	2	N/A
125	Motor Mounting Bracket	2	Plastic	Purchase	$4.99	2	N/A
126	2-56 3/8" Bolt	8	8-18 SS Steel	Purchase	$7.58	50	N/A
127	2-56 1/2" Bolt	4	8-18 SS Steel	Purchase	$8.14	50	N/A
128	#2 Lock Washer	4	8-18 SS Steel	Purchase	$2.95	100	N/A
129	#2 Washer	4	8-18 SS Steel	Purchase	$11.94	25	N/A
130	#2 Clipped Washer	8	8-18 SS Steel	Purchase	$14.40	10	N/A
131	3/8" Retaining Clip	2	1060-1090 Spring Steel	Purchase	$9.50	100	N/A
132	5/64" Allen Key	1	Steel	Purchase	$0.80	1	N/A
133	1/8" Wrench	1	Steel	Purchase	$10.79	1	N/A

134	1/4" Wrench	1	Steel	Purchase	$14.09	1	N/A
	Total:	183	N/A	N/A	$457.13	N/A	N/A

DIVERSITY, EQUITY, AND INCLUSION

Engineering decisions cannot be made in a bubble. The decisions we make as engineers have social, ethical and environmental impacts, and we must be aware of them. To determine the true impact of our design, we investigated its environmental impact, reflected on whether our stakeholder interactions demonstrated inclusive design, and contemplated on our ethical decision making throughout the design process.

Environmental Considerations

We investigated our environmental impact through the use of an eco audit utilizing GRANTA EduPack software. This tool allowed us to calculate emissions, energy expended, and cost based on materials used and manufacturing processes. The results of this analysis can be found in Fig. 24 and Table 12 below.

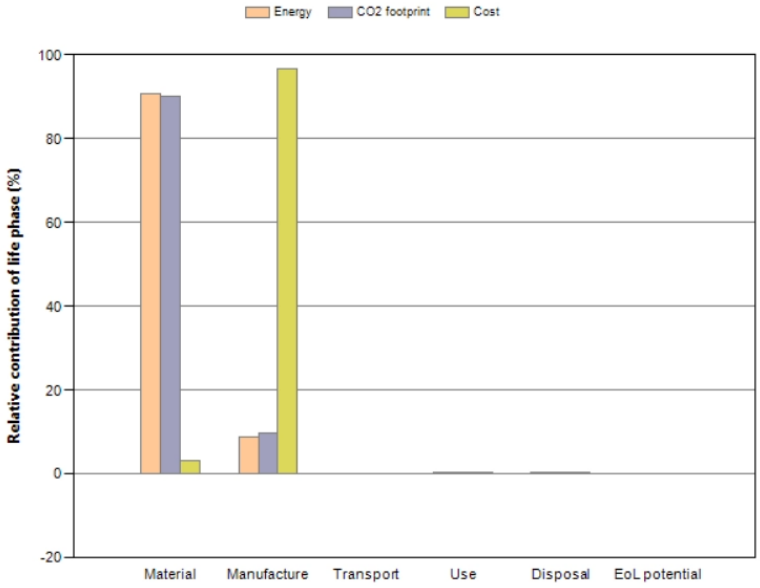

Figure 24: The graph generated through our eco audit; demonstrating that the bulk of our energy spent, emissions generated, and cost result from material and manufacture.

Table 12: A table showing the breakdown of our energy used, CO_2 footprint, and cost by phase.

Phase	Energy (kcal)	Energy (%)	CO2 footprint (lb)	CO2 footprint (%)	Cost (USD)	Cost (%)
Material	2.34e+03	90.8	1.46	90.0	0.574	3.21
Manufacture	228	8.9	0.158	9.7	17.3	96.8
Transport	0	0.0	0	0.0	0	0
Use	0.209	0.0	0.000113	0.0	3.05e-05	0.00017
Disposal	7.01	0.3	0.00453	0.3	0.000941	0.00526
Total (for first life)	**2.57e+03**	**100**	**1.63**	**100**	**17.9**	**100**
End of life potential	0		0			

To fully understand the environmental impact of our design, we chose to put our numbers into context by comparing them with the impact of a phone. Comparing our device with another similarly sized electronic device provides context by allowing us to put the environmental impact of our product in relative terms. Phones require about 0.25 gigajoules to manufacture, while according to our eco audit our device will need about 0.01 gigajoules to manufacture [21]. Additionally, the carbon footprint generated by the phone's manufacturing processes is 159 lbs [21]**.** Compared to this, the phone's carbon footprint is lower, at 1.618 lbs. Finally, we examined the cost of manufacturing both. The phone costs about $200 to make, while our compression system costs $17.90 according to GRANTA estimates[22]. Given this context, the environmental cost of our design is reasonable given its composition, size, and purpose.

The design, manufacturing, and use of our system will make progress towards a social challenge. The experiment that the device will be used to conduct will further understanding of osteoporosis, a condition that affects 200 million people [2]. In addition, the eco audit shows that there is limited potential for undesirable consequences. The device can be manufactured without difficulty, requires minimal power to operate, and is inexpensive to build. Overall, creating the device will have a positive impact.

Engineering Inclusivity Considerations

In order to practice inclusive design, the team took a number of steps. To begin, all primary stakeholders were contacted early in the project. Doing so allowed the team to fully understand their design needs and build strong requirements from the beginning. Additionally, the team sought to seek continuous feedback from the Liu Lab, with a series of meetings throughout the course of the project so far. Doing so allowed for the team to receive feedback and for both parties to provide updates and discuss next steps.

While these practices were successful, the team could have taken steps to increase its inclusivity. Communication with the other primary stakeholder, Space Tango, has been limited. Increasing communication with this stakeholder, especially at the beginning of the project, could have potentially led to stronger requirements and specifications. Doing so would also ensure that the team's work would successfully integrate into the CubeLab environment that it must use.

As shown Fig. 25, throughout the project our team has interacted with different levels of stakeholders. The primary stakeholders in our project are Liu Lab and Space Tango, as these stakeholders' work and livelihood are directly impacted by the problem at hand and our development of a design solution. The secondary stakeholders are osteoporosis patients and researchers, as these stakeholders are a part of the problem context but are not directly impacted by our design solution. The tertiary stakeholders are NASA and The University of Michigan, as these stakeholders are outside of the immediate problem contexts but are able to influence the success or failure of our design solution.

Figure 25: Stakeholder map for the project displaying stakeholders at various levels.

Engineering Ethics

In order to produce the most reliable and safe device possible for Liu Lab we conducted analysis and validation of the device. As our device will be tested upon by Liu Lab and Space Tango researchers on earth and will operate autonomously on the ISS, it is important to consider the safety of all parties involved with our device. This is especially true on the ISS, as our team does not want our device to damage any equipment within the Cube Lab or ISS; thus, components that were proven to be robust in the environment of experimentation were considered. Our team abides by the first fundamental canon within the ASME Code of Ethics of Engineers, “Engineers shall hold paramount the safety, health and welfare of the public in the performance of their professional duties” [23].

As discussed within the Environmental Considerations section of the report our team took an ethical consideration on how our design impacted the environment as a whole. For this consideration our team adhered to the eighth fundamental canon within the ASME Code of Ethics of Engineers, “Engineers shall consider environmental impact and sustainable

development in the performance of their professional duties" [23]. Analysis on this front was completed through the use of an eco audit utilizing GRANTA EduPack software.

Mechanical engineers have an ethical responsibility to provide analysis and validation results in an honest, objective way. Our project adheres to the first fundamental principle within the ASME Code of Ethics of Engineers, "Engineers uphold and advance the integrity, honor and dignity of the engineering profession by using their knowledge and skill for the enhancement of human welfare" [23]. To uphold this principle, our team adhered to be honest to our sponsors, adhere to our sponsor requirements and engineering specifications, and to be upfront with our professor, Dr. Allen Liu, so that he could help guide our decision making in an ethical and responsible way. Our main motivation to complete this project was to promote the enhancement of human welfare through any experimentation using our device that furthers knowledge into the disease of osteoporosis.

CONCLUSION

Grace Cai of Liu Lab is researching bone cell mechanics under microgravity situations. To facilitate this, bone cells will be compressed while aboard the microgravity environment of the International Space Station. In a microgravity environment, bone cells are not compressed, which artificially rapidly creates osteoporotic conditions. When bone cells are not subject to a compressive load, the necessary biochemical reactions within the body to upkeep bone structures stop. This phenomena eventually leads to osteoporosis and bone fractures to those people whose bones are under non-compressive load situations. Our team has done preliminary research on the subject of compressive loading on bone cells to understand the project's background.

To provide compression to the bone cells, Cai has asked our team to design a device capable of compressing bone cells under microgravity. Research was done to get an idea of what common characteristics cell compression devices have with one another. Three examples of cell loading devices were discussed in depth that pertain to this particular project.

The requirements of our design were determined from an interview with Grace Cai, a member of The University of Michigan Liu Lab and Lead Sponsor of the project. Cai described the desired environment of the test as well as how many individual tests are to be conducted along with a myriad other test details. A set of engineering specifications were determined to satisfy the requirements from conditions of the test stated by Cai, and the functions provided from the CubeLab box manufacturer, Space Tango. The stakeholder requirements and engineering specifications are discussed at length within the requirements and specifications section of this report.

Brainstorming sessions that explored the design solution space resulted in concept generation. From the myriad of concepts, each concept was categorized based on subfunctions of the device.

Each concept generated was evaluated through various concept evaluation techniques. Concepts that did not pass any of the evaluations were not considered for the final device design.

CAD design, computational modeling, and hand calculations were done on the design to ensure all specifications are met. Our final device design, verification, assembly procedures, and bill of materials are completed and documented. A critique of the final device design was made to document the strengths, weaknesses, and risks of the design so that potential design improvements could be made if need be. Furthermore, our team included a detailed description of project context assessment, a discussion on how our team conducted engineering inclusivity, how our team made environmental considerations, and how our team made ethical decision making when designing our device.

As the project background and definition were properly researched and project requirements were specified within Design Review 1, the future of the project was defined. For Design Review 2, the design concept exploration phase of the project occured where many design ideas were systematically narrowed down to identify one design solution. For Design Review 3, design solution development, computational modeling, and hand calculations were done to ensure all specifications were met. For the Final Solution and Project Report, all of the work from Design Review 3 was finalized, the finalized design was verified through a prototype to fulfil the requirements and specifications, and a critique of the final design was made.

Our team appreciated the opportunity given to us from Grace Cai, Liu Lab, and Space Tango to design a device that will aid the research of many.

AUTHORS

Zach Bultsma

Zach Bultsma is from Grand Rapids, MI. He is studying mechanical engineering. His favorite mechanical engineering class has been dynamics, statics and the x50 series. His interest in mechanical engineering started as a child working on vehicles with his father in the garage. Outside of school, he enjoys mountain biking, golfing, and vehicle restoration.

Rohan Dalvi

Rohan Dalvi is a mechanical engineering student from Northville, MI. His favorite mechanical engineering classes have been ME250 and statics. Outside of the classroom, he is involved with the Michigan Electric Racing team. Rohan enjoys longboarding, chess, and exploring Ann Arbor.

John Radke

John Radke is a fourth year student studying mechanical engineering. His favorite courses have been dynamics and statics. Outside of the classroom, John enjoys biking and chess. He plans to graduate in December 2021.

Sean Van Note

Sean Van Note is from Hartland, MI. He is studying mechanical engineering with a minor in economics. His favorite mechanical engineering classes have been thermodynamics, and statics. His interest in mechanical engineering started within high school while taking automotive repair, CAD, and physics classes. Outside of school, he spends his time reading books, and exercising.

REFERENCES

[1] Ohshima, H. (2017, August 7). Preventing Bone Loss in Space Flight with Prophylactic Use of Bisphosphonate: Health Promotion of the Elderly . Retrieved from https://www.nasa.gov/mission_pages/station/research/benefits/bone_loss.htm

[2] Office of the Surgeon General (US). Bone Health and Osteoporosis: A Report of the Surgeon General. Rockville (MD): Office of the Surgeon General (US); 2004. 4, The Frequency of Bone Disease. Available from: https://www.ncbi.nlm.nih.gov/books/NBK45515

[3] Osteoporosis (2019, June 19). Retrieved from https://www.mayoclinic.org/diseases-conditions/osteoporosis/symptoms-causes/syc-20351968

[4] The Dish. (2019, February 6). A New Dimension of Cell Culture: The Rise of Spheroid Culture Systems. In *Cell Culture Dish*. Retrieved from https://cellculturedish.com/cell-culture-spheroid-culture-systems/

[5]Genetos, Damian C. Pennsylvania State University. (2005). ATP release and purinergic mechanotransduction in bone cells, p. 1, 24, 64

[6]Saini, Vikas. The University of Chicago. (2006). Pulsed ultrasound and shear stress interact in their regulation of bone cell morphology and function, p. 14, 21, 37, 39

[7] Weaver, Aaron Seth. University of Michigan. (2008). The effect of mechanical stimulation on bone fracture healing: Changes in callus morphology and mesenchymal stem cell homing, p. 4, 5

[8] Joiner, Danese M. University of Michigan. (2010). The Effect of Age on Bone and its Response to Mechanical Stimulation, p. 6

[9] Ho, Kenneth Kwun Yin. University of Michigan. (2018). Progressing Mechanobiology from a Simplified to More Complex System: Development of Novel Platforms and Investigation of Actin Cytoskeletal Remodeling. Ann Arbor: ProQuest Dissertations & Theses, p. 8, 13-14, 47, 58, 74, 84, 92, 110-112

[10] Kim, Y.C., et al. Korea Advanced Institute of Science and Technology, Microfluidic biomechanical device for compressive cell stimulation and lysis.Sensors and Actuators B: Chemical, 2007. 128(1): p. 108-116

[11] Pololu Corporation. “Pololu 380:1 Micro Metal Gearmotor HPCB 6V with Extended Motor Shaft Specifications.” Las Vegas, Nevada, 6 Aug. 2015.

[12] Retrieved from https://formlabs.com/3d-printers/form-3/

[13] “Formlabs Form 2 Refurb Basic Package.” *Dynamism*, 2020, www.dynamism.com/formlabs/formlabs-3d-printers/formlabs-form2-refurbbasicpackage.html?position=&keyword=form+2&device=c&network=g&matchtype=p&campaignid=9884847528&adgroupid=100044108843&gclid=Cj0KCQjwl9GCBhDvARIsAFunhskmJcgHggaa16jKnsINbM3MAxAPHuhYDyOFWU4wy-iu9DPiuNrVKdAaAopkEALw_wcB.

[14] Fischer, T., Hayn, A. & Mierke, C.T. Fast and reliable advanced two-step pore-size analysis of biomimetic 3D extracellular matrix scaffolds. *Sci Rep* **9,** 8352 (2019). https://doi.org/10.1038/s41598-019-44764-5

[15] Serpooshan V, Quinn TM, Muja N, Nazhat SN. Hydraulic permeability of multilayered collagen gel scaffolds under plastic compression-induced unidirectional fluid flow. Acta Biomater. 2013 Jan;9(1):4673-80. doi: 10.1016/j.actbio.2012.08.031. Epub 2012 Sep 1. PMID: 22947324.

[16] Castro, A.P.G., Laity, P., Shariatzadeh, M. *et al.* Combined numerical and experimental biomechanical characterization of soft collagen hydrogel substrate. *J Mater Sci: Mater Med* **27,** 79 (2016). https://doi.org/10.1007/s10856-016-5688-3

[17] N/A. "Board of Studies, New South Wales." *Sydney Harbour Bridge*, New South Wales Education Standards Authority, 7 Aug. 2014, sydney-harbour-bridge.nesa.nsw.edu.au/engineering-studies/stress-and-strain.php.

[18] Engineering ToolBox, (2005). *Stress in Thin-Walled Tubes or Cylinders*. [online] Available at: https://www.engineeringtoolbox.com/stress-thin-walled-tube-d_948.html [Accessed 21/03/2021].

[19] Engineers Edge, (2021). *Coefficient of Friction Equation and Table Chart.* [online] Available at: https://www.engineersedge.com/coeffients_of_friction.htm [Accessed 21/03/2021].

[20] Smil, V. (2016, April 26). Your Phone Costs Energy-Even Before You Turn It On. In *IEEE Spectrum*. Retrieved from https://spectrum.ieee.org/energy/environment/your-phone-costs-energyeven-before-you-turn-it-on

[21] N/A. "Product Environmental Report IPhone 11 ." *Apple.com*, Apple, Inc., 10 Sept. 2019, www.apple.com/environment/pdf/products/iphone/iPhone_11_PER_sept2019.pdf.

[22] Larner, S. (2020, July 26). How much does an iPhone cost to make?. In *alphr*. Retrieved from https://www.alphr.com/features/388273/how-much-does-an-iphone-cost-to-make/

[23] *Society Policy: Ethics*. ASME: American Society of Mechanical Engineers, 1 Feb. 2012, www.asme.org/wwwasmeorg/media/resourcefiles/aboutasme/get%20involved/advocacy/policy-publications/p-15-7-ethics.pdf.

APPENDIX

A.1. Determination of Torque on Motor Shaft

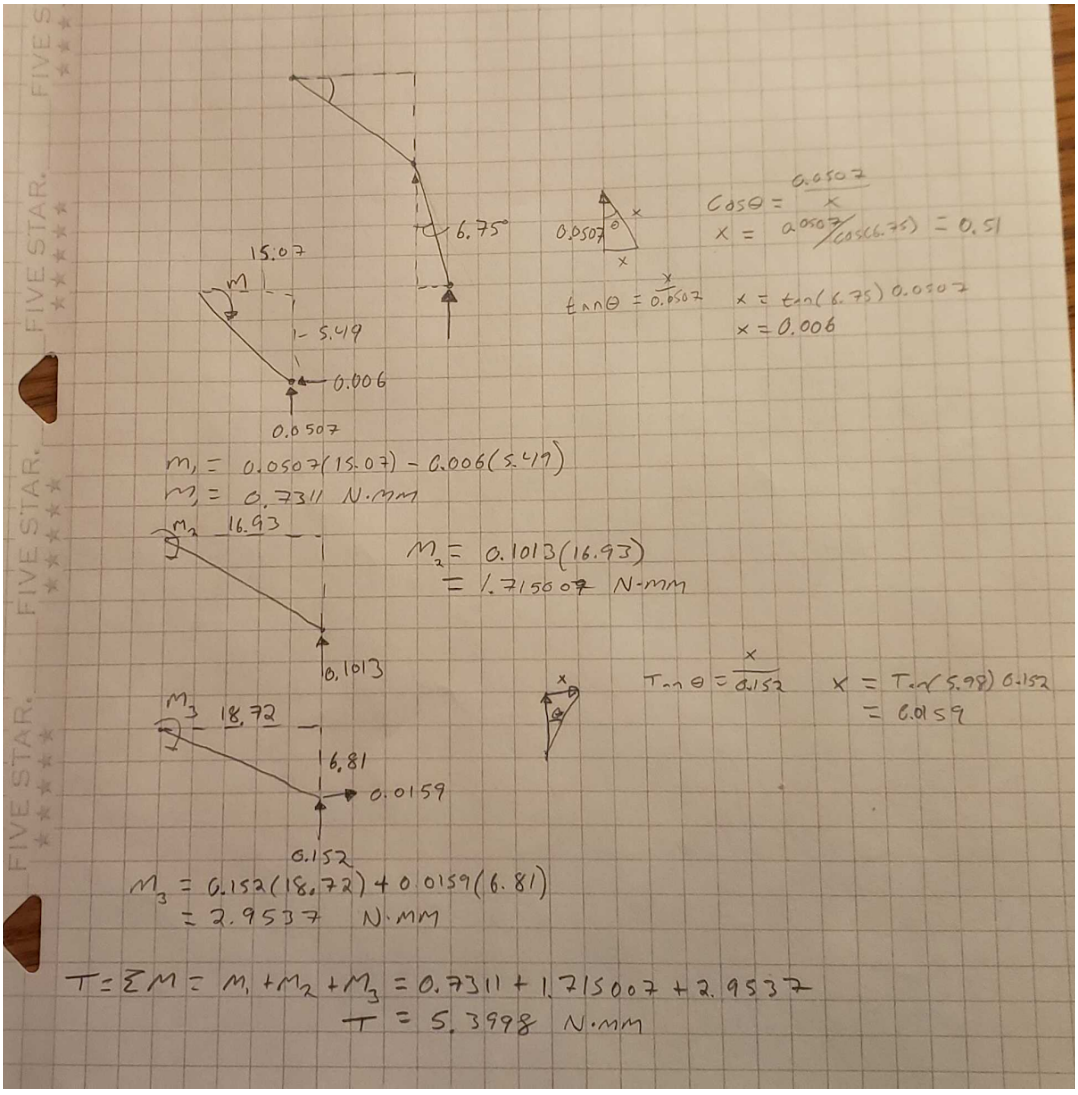

ASSEMBLY MANUAL

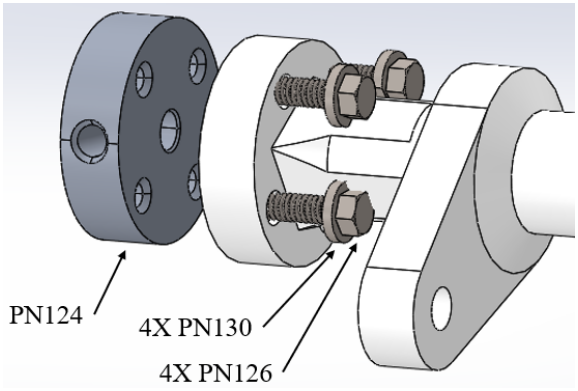

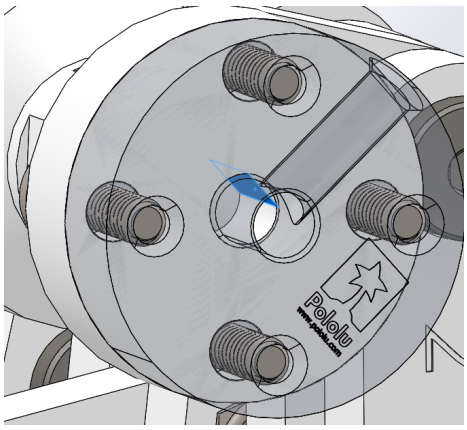

Step 1: Gather the hub (124), four bolts (126), four clipped washers (130). Ensure the set screw on the hub is perpendicular to the highlighted face. With the washer slid over the bolt and the flat face of the washer parallel to the motor shaft flat spot, insert the bolt through the hole of the motor shaft and thread into the hub by hand. Repeat this step for the remaining three bolts. Once all hand tight, use a ⅛" wrench to tighten the four bolts in a star pattern (pattern similar to attaching nuts to a car wheel).

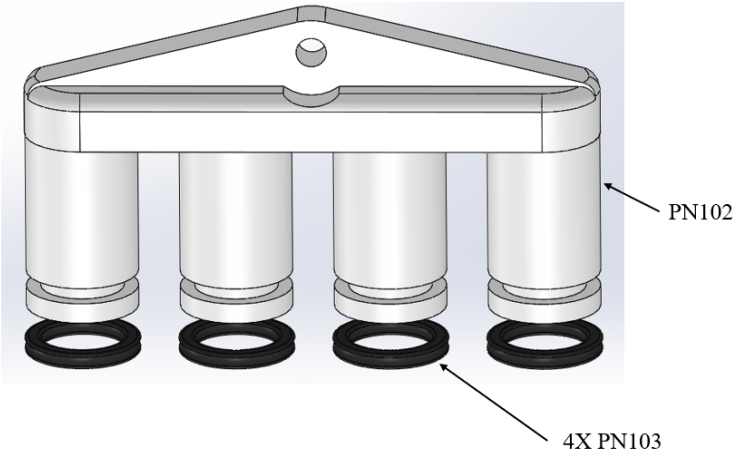

Step 2: For each piston set slip the o-ring (103) over the piston until recessed in the groove.

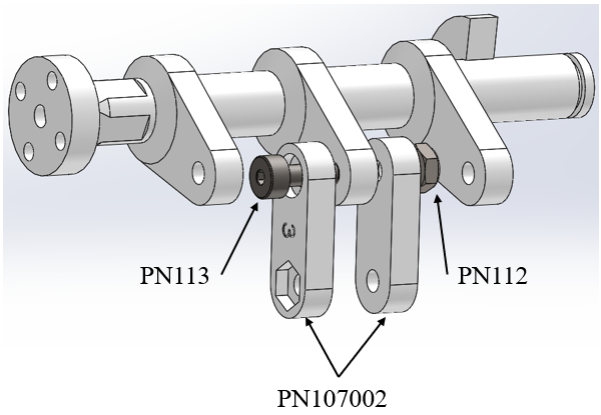

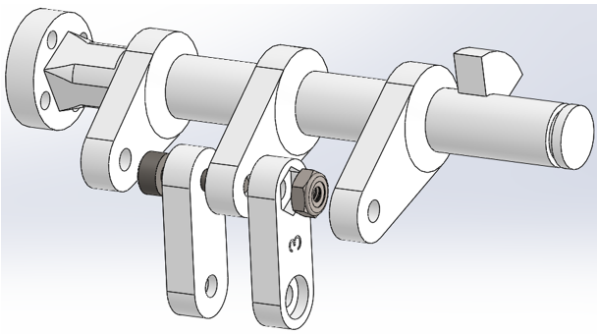

Step 3: Gather the motor shaft assembly from step 1, 2 links labeled 3 (107002), shoulder screw (113), nut (112), and the provided 5/64" allen key. With the orientation shown, place the shoulder screw through the circular end of link 3 and the hole on the cam in the middle of the motor shaft. Then use second link 3 and place the nut in the hex end. Then thread the shoulder bolt into the nut. Tighten with the allen key. Make sure the links can still rotate about the cam.

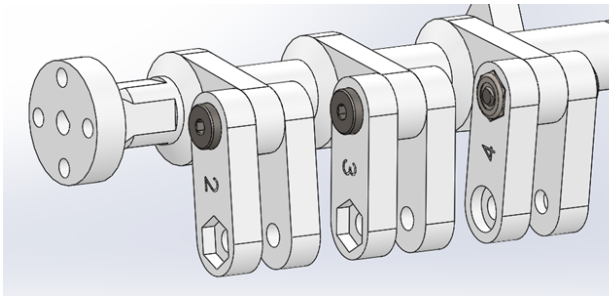

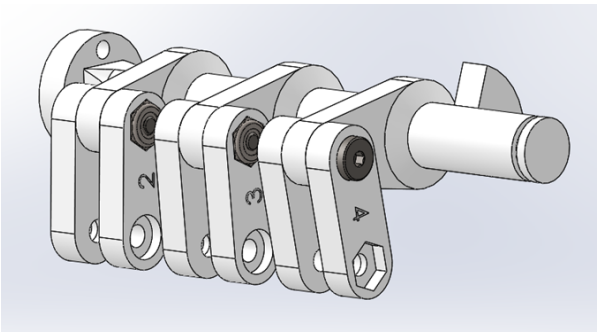

Step 4: Repeat step 3 with the links labeled 2 (107001) and 4 (107003), and the same fasteners. Make sure the bolt head is facing outwards for both 2 and 4 positions. In other words, attach the fasteners in the same orientation as shown in the two figures above.

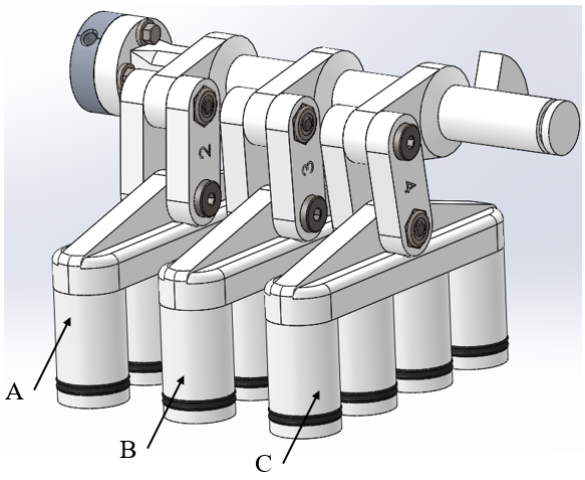

Step 5: With the same fasteners as step 3, take the pistons assembled in step 2 and attach them to the bottom of each link. It may be easier to start at piston row A then work your way to piston row C.

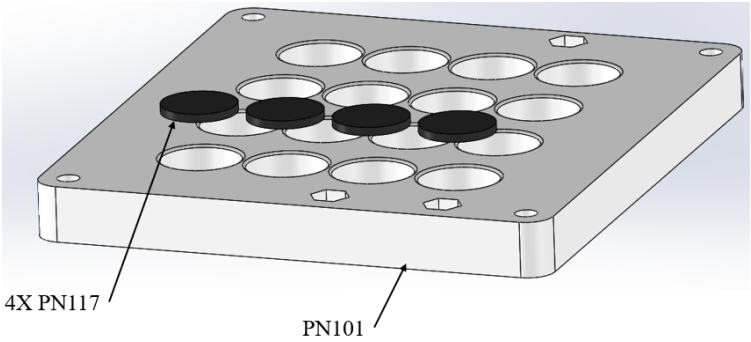

Step 6: Take four gaskets (117) and place them into the row of cylinders closest to the two hexagonal indentations with glue in between the gasket and cylinder housing (101). Make sure to let the glue dry for an appropriate amount of time.

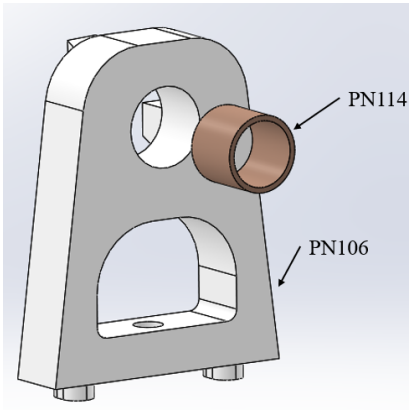

Step 7: Gather the sleeve bearing (114) and pillow block (106). Place the bearing into the large hole on the pillow block. To fix any bearing movement within hole, use glue between the bearing and hole.

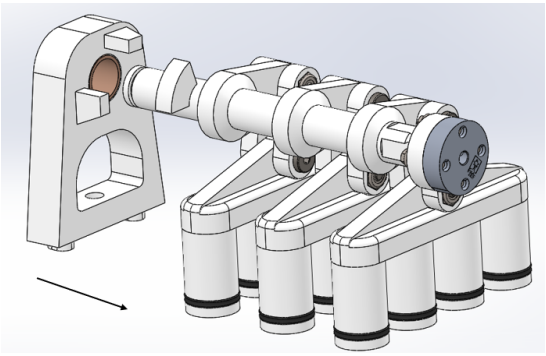

Step 8: Gather the assemblies from Step 5 and Step 7. Slide the pillow block onto the motor shaft as shown. Then, place the retaining clip (131) onto the cut out of the motor shaft once the cut out is visible through the other side of the pillow block.

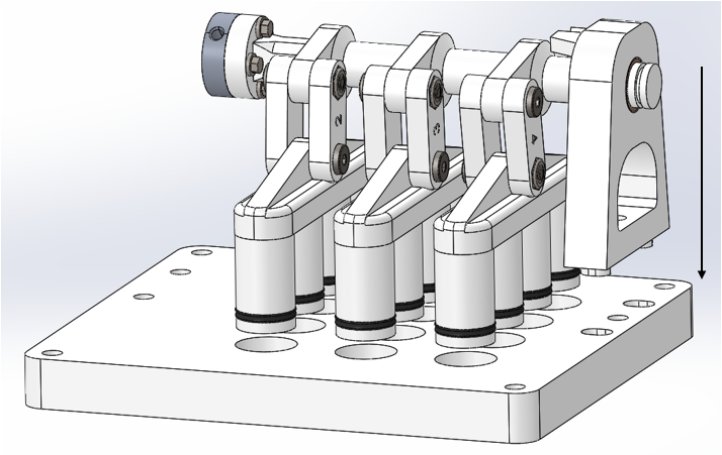

Step 9: Gather the assemblies from Step 6 and Step 8. Slide the pistons through the cylinder housing holes and make sure the pillow block falls into the recesses.

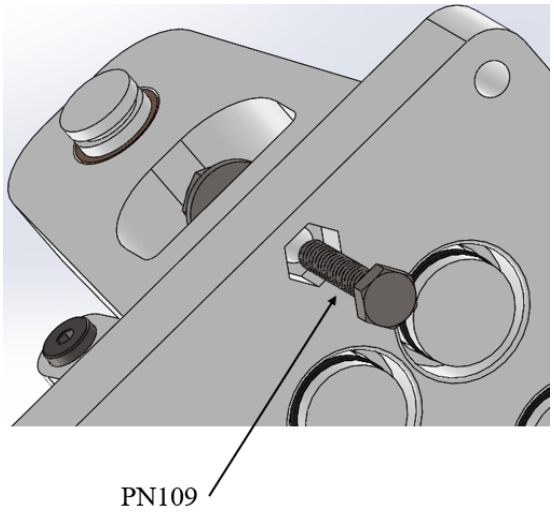

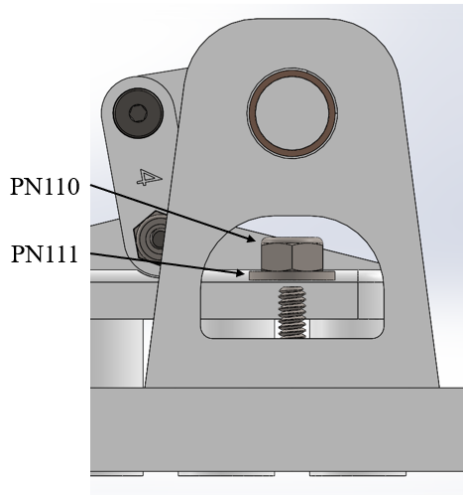

Step 10: With the pillow block, linkage, and pistons on the cylinder housing plate, slide a bolt (109) up through the hole shown, then place a washer (111) on the bolt and thread the nut (110) down. Tighten to snug with a 5/16” wrench.

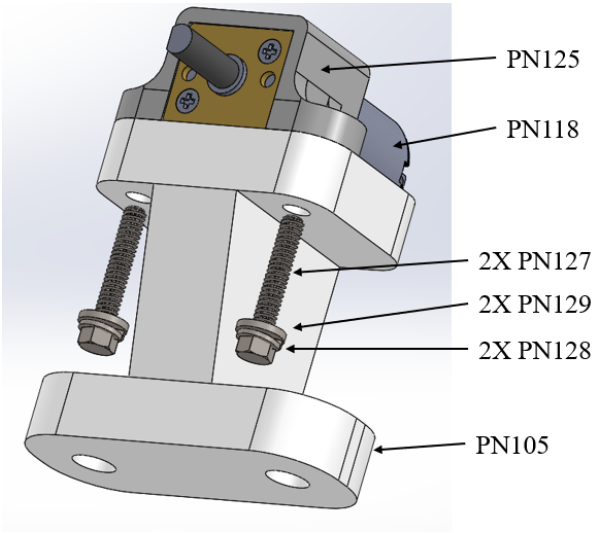

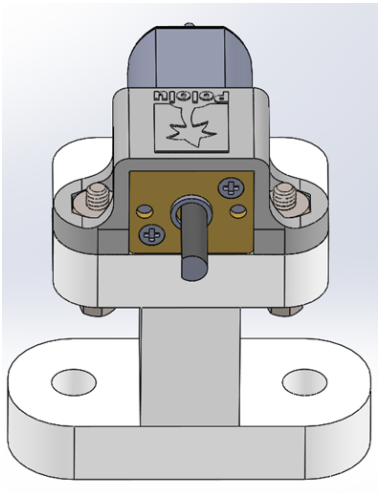

Step 11: Gather the pillow block for the motor (105), motor (118), motor bracket (125), two bolts (127), two lock washers (128), and two washers (129). Place the nuts included with the motor bracket into the space on the motor bracket, then place the motor in the bracket in the orientation shown. With the bolt, lock washer, and washer (stacked in that order), place through the hole of the pillow bolt and thread into the nut. Use a 1//8” wrench to tighten.

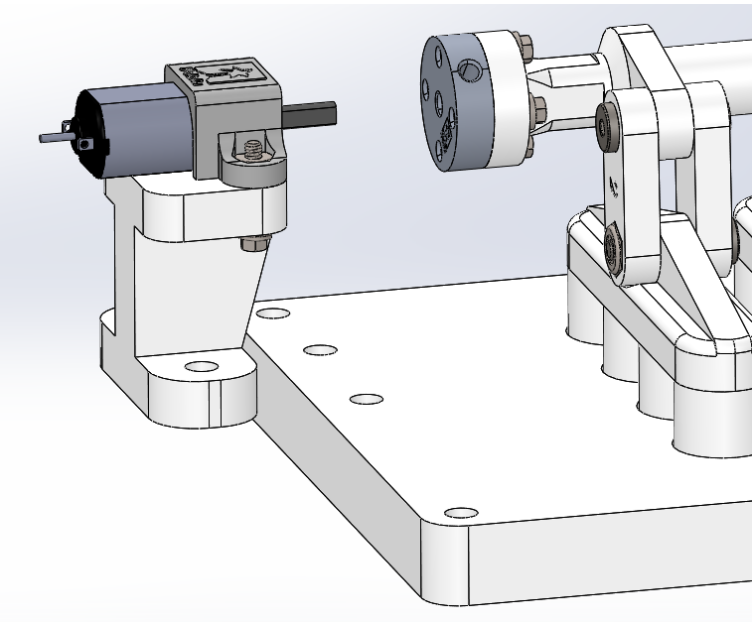

Step 12: Gather the assemblies from Steps 10 and 11. With the flat spot of the motor's shaft (grey shaft protruding out of the motor) perpendicular to the set screw on the hub, slide the motor's shaft into the hub until the motor pillow block holes are aligned with the cylinder plate holes.

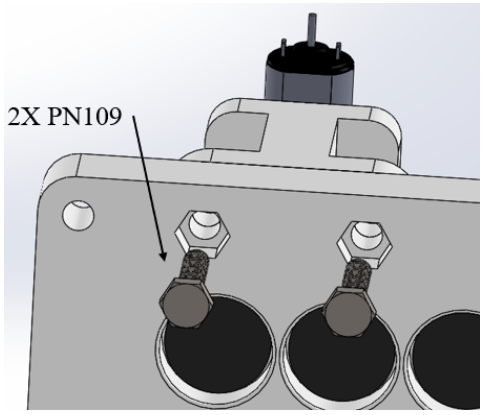

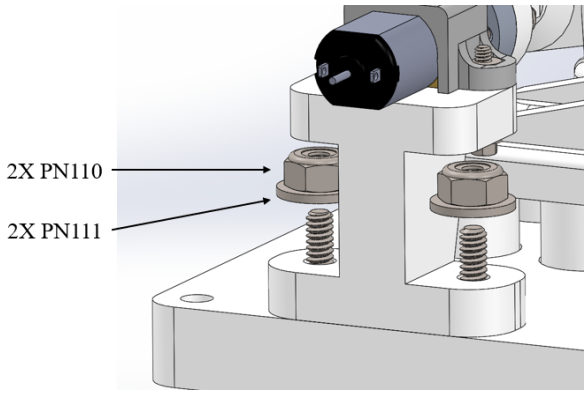

Step 13: Place two bolts (109) through the holes shown lining up the hex features. Then place the washer (111) over the bolt and thread the nut (110) as shown. Tighten with a 5/16" wrench.

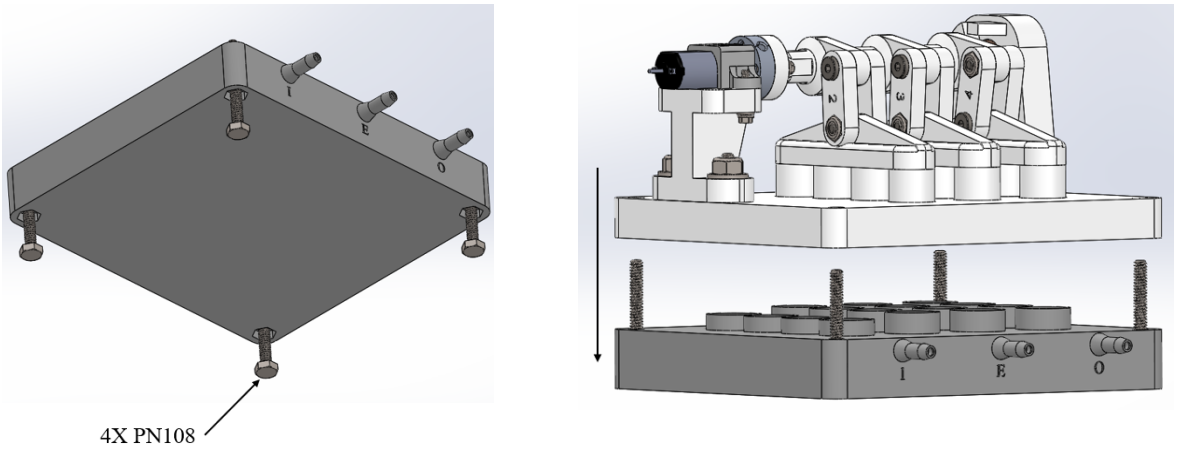

Step 14: Gather four bolts (108) and place them through the holes in the corners of the base plate. Then slide the assembly from step 13 on the base plate.

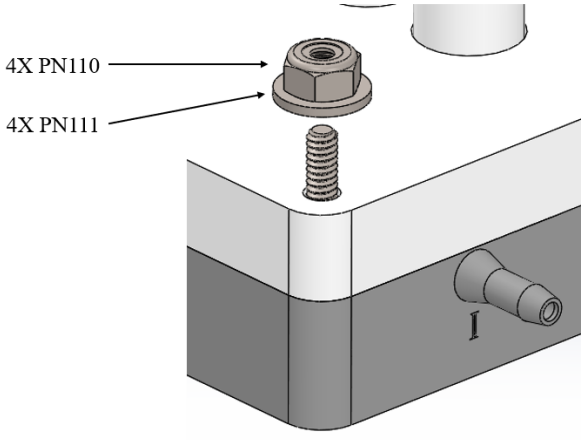

Step 15: In each corner, put a washer (111) over the bolts and thread on a nut (110). Tighten with a 5/16” wrench.